Available online at www.sciencedirect.com

ScienceDirect

Geochimica et Cosmochimica Acta 257 (2019) 336–353

Geochimica et Cosmochimica Acta

www.elsevier.com/locate/gca

Aqueous alteration of pyroxene in sulfate, chloride, and perchlorate brines: Implications for post-Noachian aqueous alteration on Mars

Charity M. Phillips-Lander[a], Andrew S. Elwood Madden[a], Elisabeth M. Hausrath[b], Megan E. Elwood Madden[a]

[a] *School of Geology and Geophysics, University of Oklahoma, 100 E. Boyd Street, Norman, OK 73069, USA*
[b] *Department of Geoscience, University of Nevada, Las Vegas 4505 S. Maryland Ave., Las Vegas, NV 89154, USA*

Received 14 August 2018; accepted in revised form 6 May 2019; available online 11 May 2019

Abstract

Both high and low calcium pyroxene minerals have been detected over large portions of the martian surface in addition to widespread salts in martian soils and dust. Calcium pyroxenes in martian meteorites are associated with secondary evaporite phases, including sulfates, chlorides, and perchlorates, suggesting the pyroxene may have been altered in saline solutions. Therefore, understanding pyroxene mineral weathering in high salinity brines may provide insight into past aqueous alteration on Mars. This study examines both solute-based dissolution rates and qualitative assessments of weathering textures developed during pyroxene-brine alteration experiments to link dissolution rates and textures and aid in interpreting weathering features observed in Mars meteorites and future pyroxene samples returned from Mars. Batch reactor dissolution experiments were conducted at 298 K to compare diopside (a high Ca-pyroxene) dissolution rates in water (18 $M\Omega\ cm^{-1}$ ultrapure water (UPW); activity of water ($\alpha H_2O = 1.0$), 0.35 $mol\ kg^{-1}$ NaCl ($\alpha H_2O = 0.99$), 0.35 $mol\ kg^{-1}$ Na_2SO_4 ($\alpha H_2O = 0.98$), 2 $mol\ kg^{-1}$ $NaClO_4$ ($\alpha H_2O = 0.90$), 2.5 $mol\ kg^{-1}$ Na_2SO_4 ($\alpha H_2O = 0.95$), 5.7 $mol\ kg^{-1}$ NaCl ($\alpha H_2O = 0.75$), and 9 $mol\ kg^{-1}$ $CaCl_2$ ($\alpha H_2O = 0.35$) brines at pH 5–6.6 to determine how changing solution chemistry and activity of water influence pyroxene dissolution. Aqueous Si release rates and qualitative textural analyses indicate diopside dissolution rates are influenced by both solution chemistry and activity of water, with diopside weathering increasing along a trend from: 9 $mol\ kg^{-1}$ $CaCl_2 <$ UPW (-9.82 ± 0.03 log $mol\ m^{-2}\ s^{-1}$) $\approx$ 2 $mol\ kg^{-1}$ $NaClO_4 \approx$ 0.35 $mol\ kg^{-1}$ Na_2SO_4 (-9.80 ± 0.07) $\approx$ 5.7 $mol\ kg^{-1}$ NaCl (-9.69 ± 0.04) $<$ 0.35 $mol\ kg^{-1}$ NaCl (-9.45 ± 0.34) $<$ 2.5 $mol\ kg^{-1}$ Na_2SO_4 (-8.99 ± 0.09). Dissolution rates increase in sodium sulfate brines with increasing salinity. In contrast, Si-based dissolution rates in 0.35 $mol\ kg^{-1}$ NaCl are faster than those measured in 5.7 $mol\ kg^{-1}$ NaCl and UPW. However, all of the Si-based rates measured in the chloride and sulfate salt solutions are likely affected by precipitation of Si-rich secondary clay minerals, which removed Si from solution. Qualitative textural analyses indicate similar degrees of dissolution occurred in UPW and 2 M $NaClO_4$; however, no aqueous rate determinations could be made in perchlorate brines due to explosion hazards. Aqueous Si was below detection limits in the 9 $mol\ kg^{-1}$ $CaCl_2$ experiments, but textural analysis suggests limited diopside dissolution occurred. Therefore, despite low water activity, diopside dissolution proceeds in both dilute to high salinity brines, readily forming clay minerals under a wide range of conditions. This suggests that outcrops on Mars containing pyroxene preserved with sulfate, chloride, perchlorate, and/or clay minerals likely record relatively short periods (<1 million years) of aqueous alteration. Si-rich spher-

---

E-mail address: melwood@ou.edu (M.E. Elwood Madden)

https://doi.org/10.1016/j.gca.2019.05.006

ules similar to those observed in SNC meteorites were also observed in the 5.7 mol kg^{-1} NaCl brine experiments, indicating that silicate mineral alteration in chloride brines may lead to Si-rich alteration products and coatings.

Keywords: Pyroxene; Weathering; Mars; Chloride; Sulfate; Perchlorate

1. INTRODUCTION

Pyroxene minerals have been detected on Mars by both orbital and rover observations (e.g. Christensen et al., 1998; Mustard et al., 2005; Bibring et al., 2006; Mustard et al., 2007; McSween et al., 2008; Blake et al., 2013; Vaniman et al., 2013) and within SNC meteorites (e.g. Treiman, 2005; Velbel and Losiak, 2010; Velbel, 2012). Compact Reconnaissance Imaging Spectrometer for Mars (CRISM), Thermal Emission Spectrometer (TES), and Observatoire pour la Mineralogie, l'Eau, les Glaces et l'Activité (OMEGA) data indicate pyroxenes are present in ancient and volcanic terrains in the southern highlands as well as in polar dune fields on Mars (Bandfield et al., 2000; Bibring et al., 2005, 2006). Pyroxene was inferred from geochemical measurements of basalts by Pathfinder's Alpha Particle X-ray Spectrometer (APXS, McSween et al., 2004) and identified in rocks and soils by the Mössbauer Spectrometer on Spirit and Opportunity (Morris et al., 2004, 2006, 2008). Opportunity also detected 5–15% pyroxenes in weathered soils at Meridiani Planum by mini-TES (Christensen et al., 2004; Klingelhöfer et al., 2004). Pyroxene minerals have also been detected in both modern eolian sediments and ancient sedimentary rocks in Gale crater by the CheMin X-ray diffraction instrument on the Mars Science Laboratory rover (Blake et al., 2013; Bish et al., 2013; Vaniman et al., 2013; Treiman et al., 2016; Achilles et al., 2017; Rampe et al., 2017; Yen et al., 2017; Bristow et al., 2018; Rampe et al., 2018).

Martian pyroxenes have diverse chemical compositions (Mustard et al., 2005); from orbit low-calcium pyroxenes (LCP) are primarily associated with Noachian-aged exposures; however, high-calcium pyroxenes (HCP) are typically detected and are common in Hesperian-aged terrains where both LCP and HCP are observed in 40:60 mixtures (Mustard et al., 2005). High-calcium pyroxenes are enriched in martian dune features (Mustard et al., 2005; Langevin et al., 2005), Syrtis Major, upper layers of Juventae Chasma and Coprates Chasma (Mustard et al., 2005), and the southern highland regions (Bandfield, 2002). Active eolian sands in the Bagnold Dune Field in Gale crater contain variable amounts of augite and pigeonite (Achilles et al., 2017; Rampe et al., 2018), and augite, pigeonite, and orthopyroxene have been reported in drilled sedimentary rock samples from Gale crater (Blake et al., 2013; Bish et al., 2013; Vaniman et al., 2013; Treiman et al., 2016; Achilles et al., 2017; Rampe et al., 2017; Yen et al., 2017; Bristow et al., 2018; Rampe et al., 2018).

The SNC meteorites represent basaltic and ultramafic composition igneous rocks derived from Mars, and all contain pyroxene (e.g. Nyquist et al., 2001). Similar LCP:HCP ratios are also common in SNC meteorites (McSween, 2002). Shergottites consist primarily of pyroxene and plagioclase minerals, reflecting their basaltic and lherzolitic compositions (McSween, 1994; Harvey et al., 1993). The nakhalites are clinopyroxenite meteorites consisting primarily augite and pigeonite (Gooding et al., 1991; Bridges and Grady, 2000; Treiman, 2005; Bridges and Warren, 2006). In contrast, Chassigny meteorites consist primarily of olivine with minor (~5%) pyroxene (Floran et al., 1978). ALH84001 is significantly different than the rest of the SNC meteorites as it contains approximately 96% orthopyroxene (Mittlefehldt, 1994).

In addition to pyroxene minerals, chloride and sulfate salts have been detected in several Mars meteorites. Sulfate and chloride salts occur as coatings on fracture surfaces and as discontinuous veins in primary minerals, including pyroxene, in Chassigny (Wentworth and Gooding, 1994) and MIL 03346 (Ling and Wang, 2015) meteorites. While some salts may be of terrestrial origin, sulfate salts are intergrown with smectite in Nakhla and have been interpreted to represent water-rock interactions on Mars (Gooding et al., 1991) and S and Cl are adsorbed to secondary clay minerals and Fe-oxides in Lafayette (Treiman et al., 1993). These data suggest, in some instances, episodic weathering of pyroxene minerals in circum-neutral to high pH saline waters on or near Mars' surface (Lee et al., 2015; Velbel, 2012; Treiman et al., 1993; McSween, 1994).

Chloride and sulfate salts have also been observed in association with pyroxenes in a variety of different terrains on the surface of Mars. For example, martian soils are composed of loose silicate-salt matrices, with variable chloride and sulfate enrichments (Archer et al., 2014; Amundson et al., 2008). In many instances pyroxenes have been observed with salts, including LCP associated with sulfate salts in Meridiani Planum (Squyres et al., 2004) and HCP associated with sulfate minerals observed in drill powders collected from John Klein and Cumberland in Gale crater (Vaniman et al., 2013). In addition, weathered basalts are associated with high concentrations of sulfate and chlorine in Gusev Crater (Haskin et al., 2005). OMEGA data indicate pyroxene is associated with sulfate salts in dunes in the north polar region (Bibring et al., 2006). XRD analyses of Murray mudstone samples in Gale Crater also show both pyroxene and secondary weathering products (primarily hematite, calcium sulfates, and clay minerals, as well as halite in Quela), but the presence of mafic primary minerals appears to be anticorrelated with the secondary products, suggesting chemical weathering occurred (Bristow, 2018). Chloride salts appear to be associated with phyllosilicates (Osterloo et al., 2008, 2010) in Noachian terrains, and have been observed in several martian meteorites.

The abundance of salt deposits combined with the low-atmospheric pressure and low temperature conditions at or near Mars's surface suggest that many post-Noachian chemical weathering processes likely occurred in briny solutions. The presence of salts associated with HiRISE observations of recurring slope lineae indicates ephemeral melting of ices and the formation of high ionic strength brines may occur on the surface of Mars today (e.g. Mitchell and Christensen, 2016; Ojha et al., 2015, 2014; McEwen et al., 2014, 2011). HiRISE images show surface features including dark spots on dunes (Martínez et al., 2012) and flow-like features (Möhlmann and Kereszturi, 2010) that also indicate the presence of ephemeral liquid brines. Perchlorate (Rennó et al., 2009; Kounaves et al., 2010a) and sulfate (Kounaves et al., 2010b) salts were also observed in the subsurface by the Phoenix lander. Perchlorate has also been detected in many samples in Gale crater by the Sample Analysis at Mars (SAM) instrument (e.g., Sutter et al., 2017). These brines ($NaClO_4$-$CaCl_2$-NaCl-H_2O) likely remain liquid at temperatures below −50 °C, which would promote chemical weathering at or near Mars's surface (e.g. Hausrath and Brantley, 2010; Niles et al., 2017, Toner and Catling, 2017).

However, despite the likely importance of brines to weathering on Mars, previous research investigating pyroxene dissolution rates has focused primarily on dilute solutions. Pyroxene dissolution is dependent on pH and T in dilute solutions (Chen and Brantley, 1998; Hoch et al., 1996; Knauss et al., 1993; Schott et al., 1981; Golubev et al., 2005). The effect of pyroxene composition on mineral dissolution rates is difficult to study due to their widely varying compositions (see Brantley, 2003; Bandstra and Brantley, 2008; Chen and Brantley, 1998; Eggleston et al., 1989; Hoch et al., 1996; Knauss et al., 1993; Schott et al., 1981; Golubev et al., 2005). However, trends in the behavior of different elements in dissolution suggest that Ca and Fe-containing pyroxenes would likely dissolve more rapidly than Ca/Mg or Ca-dominant pyroxenes which would dissolve more rapidly than Mg-dominant pyroxenes (Brantley, 2003; Brantley and Olsen, 2014). Oxidation of Fe within the pyroxene mineral structure is also expected to enhance dissolution rates; however this factor is greatest at low pH (White and Yee, 1985; Hoch et al., 1996). Diopside ($CaMgSi_2O_6$) dissolution rates have also been shown to be unaffected by pCO_2 up to ~1 atm, and the presence of carbonate and bicarbonate ions (CO_3^{2-}, HCO_3^-) at 0.1 M concentrations (Golubev et al., 2005).

Prior studies have demonstrated that initial pyroxene dissolution is incongruent, leading to preferential release of cations into solution and the formation of a constant-thickness, cation-depleted surface layer (Schott et al., 1981; Schott and Berner, 1985). This model predicts that the dissolution rate is linked to the activity of the leached cation(s) in solution (Oelkers and Schott, 2001). Daval et al. (2010) demonstrated that increased aqueous silica concentration resulted in slower diopside dissolution rates. In silica-undersaturated solutions, cations are leached from the surface forming an amorphous Si-rich layer, which is unstable and dissolves (Daval et al., 2013). This process continues until Si-saturation is reached in the solution.

In addition, other background electrolytes also influence silicate dissolution rates. Previous studies of mineral dissolution in brines indicate mineral dissolution rates in chloride brines often decrease with decreasing activity of water (Elwood Madden et al., 2017; Miller et al., 2016; Steiner et al., 2016; Olsen et al., 2015; Pritchett et al., 2012). However, previous studies of quartz and carbonate mineral dissolution at circum-neutral pH indicate both cations and anions present in solution influence mineral dissolution rates and rate trends (Phillips-Lander et al., 2018; Ruiz-Agudo et al., 2009; Gledhill and Morse, 2006; Arvidson et al., 2006; Dove, 1999; Dove and Nix, 1997).

This study seeks to measure pyroxene dissolution rates as a function of brine composition and water activity. To investigate these relationships, we reacted diopside, a calcium-rich pyroxene relevant to HCP on Mars, with ultrapure water (UPW); low salinity brines including 0.35 mol kg^{-1} NaCl ($aH_2O = 0.99$), 0.35 mol kg^{-1} Na_2SO_4 ($aH_2O = 0.98$), and 2 mol kg^{-1} $NaClO_4$ ($aH_2O = 0.9$); and near-saturated 5.7 mol kg^{-1} NaCl ($aH_2O = 0.75$), 2.5 M Na_2SO_4 ($aH_2O = 0.95$), and 9 mol kg^{-1} $CaCl_2$ ($aH_2O = 0.35$). Experiments were conducted at 25 °C for approximately 60 days. Calcium, magnesium, and iron released from the pyroxene were measured with atomic absorption spectroscopy (AAS). Silicon release was measured using UV–visible (UV–Vis) absorption spectroscopy. Solid reaction products were analyzed with X-ray diffraction (XRD) and provide insights into the association between salts and secondary weathering products on Mars. Alteration textures were observed using scanning electron microscopy (SEM) and clay precipitates analyzed with energy dispersive X-ray microanalysis (EDXA).

2. METHODS

2.1. Pyroxene Characterization

A sample of diopside ($Ca_{0.96}$,$Na_{0.04}$,$Fe_{0.33}$,$Mg_{0.65}$,$Al_{0.04}$)$Si_{1.9}O_6$, a Ca-rich pyroxene, was obtained from Wards Scientific (#466474, Phillips-Lander et al., 2017). The diopside was crushed to <1 mm grain size using an agate mortar and pestle, then ground to ~30 micron-sized particles using a McCrone mill, sonicated in ethanol to clean mineral surfaces prior to reaction, and air-dried. Unreacted pyroxene particle size was verified by scanning electron microscopy. Specific surface area was measured using a Quantachrome Nova 200e BET surface area analyzer using nitrogen adsorption following degassing at 50 °C for 12 h. The surface area of the crushed diopside starting material was $0.49 \pm 0.05\ m^2\ g^{-1}$.

Bulk mineralogy of the powdered sample was determined using a Rigaku Ultima IV X-ray diffractometer, Cu tube at 40 kV and 44 mA, diffracted beam monochromator monochromator, and MDI Jade 2010 software for data interpretation. Whole pattern fitting of the XRD data indicated the presence of minor biotite, amphibole, and zeolite (~1% each) with diopside in the unreacted material, which was not observed in previous electron probe analysis (Phillips-Lander et al., 2017).

2.2. Dissolution rate experiments

Batch experiments were conducted in triplicate with 1 g diopside per L solution using 18 MΩ cm^{-1} water (UPW), low-salinity brines 0.35 mol kg^{-1} NaCl (aH$_2$O = 0.99), 0.35 mol kg^{-1} Na$_2$SO$_4$ (aH$_2$O = 0.98) and near-saturated 5.7 mol kg^{-1} NaCl (aH$_2$O = 0.75), 2.5 mol kg^{-1} Na$_2$SO$_4$ (aH$_2$O = 0.95), and 9 mol kg^{-1} CaCl$_2$ (aH$_2$O = 0.35) brines at 25 °C, using the same reactors and methods employed by Elwood Madden et al. (2012). These batch experiments approximate closed-system alteration environments and may therefore be relevant to weathering conditions observed similar martian environments including Yellowknife Bay, Gale Crater (Vaniman et al., 2013; McLennan et al., 2013).

We used Na-salts to ensure we would be able to measure Ca, Mg, and Fe cations released from diopside to solution. We included CaCl$_2$ brine experiments as a reference point for solutions with low activities of water and because recent studies have shown CaCl$_2$-brines are associated with water tracks in the McMurdo Dry Valleys, a Mars analog (Gough et al., 2016). Similar brines have been included in a variety of Mars analog weathering studies (e.g. Hausrath and Brantley, 2010; Pritchett et al., 2012; Phillips-Lander et al., 2017; Phillips-Lander et al., 2018). Each experimental batch reactor contained 0.1 g of powdered pyroxene and 100 mL of solution, which were stirred with a Teflon-coated stir bar on a stir plate operating at 120 rpm to keep the mineral powder suspended for 60 days. We measured the pH in a subsample of the initial experimental solution, since initial dissolution rates may vary with initial solution pH, but did not measure pH in subsequent samples due to challenges measuring pH accurately in small samples of high salinity brines.

We retrieved a 10 mL aliquot of mineral solution slurry at weekly intervals. We filtered the solution slurry through a 0.2 μm acetate syringe filter into a sample tube. After collection, samples were acidified with 1 mL of 50% v/v high purity nitric acid and stored in a refrigerator at 4 °C until analysis. This method of filtering, then acidifying the samples is commonly used in mineral dissolution studies, but can result in variations in the observed "solute" concentrations due to colloids <0.2 μm passing through the filter, then dissolving due to acidification. Therefore, the solute data presented likely represents both solutes and colloidal material <0.2 μm. At the end of each experiment, we filtered the remaining solids onto 0.2 μm acetate filter paper and rinsed the solids with ultrapure water 3 times while vacuum filtering the samples.

Dissolved Ca, Mg, Fe, and K were measured in each aliquot using a Perkin Elmer AAnalayst800 flame AAS. Matrix-matched standards were used to construct calibration curves. Absorbance was measured three times and averaged. Because measuring solutions that contain such high concentrations of salts is technically challenging, we took a variety of steps to both enable the analysis and protect our instrumentation – we detail these steps here for others who might wish to perform such analyses. To ensure accurate analyses, we diluted each sample with ultrapure water to prevent clogging of the AAS nebulizer. We further ensured maximum analytical accuracy by flushing the system with ultrapure water between each sample analysis and 0.1% Triton-X detergent between each sample set. At the end of each day, we removed the burner head, thoroughly rinsed and soaked it overnight. We flushed the AAS drain tube with ultrapure water to prevent salt accumulation in the system.

We measured dissolved Si in solution using UV–Vis adsorption spectroscopy following Steiner et al.'s (2016) methyl-blue method modified for use with brines. We attempted to measure dissolved Al using UV–Vis; however, we could not construct useful calibration curves in the high salinity brines.

2.2.1. Dissolution rate determination

We first subtracted a matrix blank from the solution concentrations to correct for any background cations in the brines. The data in Supplemental Table 1 represent the concentration data after the background concentration for each experiment was subtracted. We determined the surface area-normalized dissolution rate (mol m^{-2} s^{-1}) by dividing the concentration of each cation by the measured BET surface area and then plotting these data versus time. We determined the initial dissolution rates for each experiment by fitting the first five data points of the surface area normalized dissolution data versus time plots using a linear regression and calculating the slope of the line to determine the dissolution rate.

Due to the presence of minor biotite (<1–2 wt%) observed during XRD analysis, we measured aqueous K to assess the potential impact of biotite dissolution on measured Si-based dissolution rates. While most of the K released to solution is likely due to cation exchange reactions, without wholescale biotite dissolution, we calculated the amount of Si released from biotite due to congruent dissolution based on the K release rates. Our analysis indicated that even the maximum potential Si-contribution from biotite dissolution was minimal (Supplemental Table 1). In addition, amphibole (Schott et al., 1981) and zeolite (Ragnarsdóttir, 1993; Savage et al., 2001; Cotton, 2008; Glover et al., 2010) dissolution rates are significantly slower than diopside dissolution rates and likely did not contribute significantly to aqueous Si release. Therefore, we elected to report the rates as the total Si released to solution.

2.3. Microscopy-based qualitative assessment of pyroxene dissolution

We conducted a second set of experiments to qualitatively assess diopside weathering textures on larger particles using scanning electron microscopy. These experiments also allowed us to examine dissolution in 2 mol kg^{-1} NaClO$_4$ brine, which we could not use for aqueous analyses due to the explosion risks in the flame AAS. We crushed, sieved (2–4 mm size fraction), sonicated in ethanol, and air-dried diopside before adding the pyroxene to each experimental solution at a 1 g L^{-1} ratio. We used the same experimental solutions used in the aqueous dissolution experiments (i.e. UPW, 0.35 mol kg^{-1} NaCl, 0.35 mol kg^{-1} Na$_2$SO$_4$, 5.7 mol kg^{-1} NaCl, 2.5 mol kg^{-1} Na$_2$SO$_4$, and 9 mol kg^{-1} CaCl$_2$) in addition to 2 mol kg^{-1} NaClO$_4$ (aH$_2$O = 0.90). We placed each batch reactor on an orbital shaker table at 120 rpm for 60 days. Upon completion of the experiments, we collected the solids and triple rinsed them in ultrapure water, then left them to air-dry for 24 h. Samples were mounted on SEM stubs and iridium-coated for SEM analysis. We collected images of the unreacted diopside, as well as diopside dissolution textures from the weathering experiments using a Zeiss Neon FEG-SEM located at the University of Oklahoma's Sam Noble Microscopy Laboratory.

We evaluated the degree of weathering by examining no fewer than 20 images from each weathering experiment at 10–100 nm scales and comparing them to SEM images of unreacted grains. Qualitative weathering was ranked using a (−) to (+++) scale which indicates the extent of dissolution based on observations of etch pits, denticles, and clay minerals. We also estimated percent clay mineral coverage.

2.4. Reaction products characterization

Upon completion of aqueous dissolution experiments, the remaining solutions were decanted, filtered through a 0.2 μm filter, acidified to 1% v/v, and stored at 4 °C. Remaining solid material was rinsed with 18 MΩ cm^{-1} water to remove any salts and air-dried. The reaction products were analyzed using powder X-ray diffraction on a Rigaku Ultima IV with a Cu-tube at 40 kV and 44 mA, with a diffracted beam monochrometer and scintillation detector. Data interpretation was conducted with MDI Jade (2010). We also assessed the chemistry of reaction products observed during SEM analysis using the Zeiss NEON FEG-SEM, which is equipped with an INCA Energy 250 Energy Dispersive X-ray (EDXA) microanalysis system. We normalized the Ca, Fe, Mg, Al, and Si data to 100% and plotted them on a ternary plot to compare the chemical composition of the clay minerals with the starting material.

3. RESULTS

3.1. Aqueous analyses

Si, Mg, and Fe concentrations in the 9 mol kg^{-1} $CaCl_2$ experiments were below detection limits and, as previously noted, we did not analyze the solutes in the $NaClO_4$ experiment due to explosion risks. Therefore, we only report aqueous data from the UPW, NaCl, and Na_2SO_4 experiments. Ca, Mg, Fe and Si concentrations varied slightly between experimental trials (Supplemental Table 1) but followed similar trends; representative dissolution data from each experimental condition are shown in Fig. 1.

Based on the initial Si-release rates (Fig. 2, Table 1), we observe that pyroxene appears to release Si to solution fastest in the 2.5 mol kg^{-1} Na_2SO_4 brine (-8.98 ± 0.09 log mol m^{-2} s^{-1}), followed by 0.35 mol kg^{-1} NaCl (-9.15 ± 0.06 log mol m^{-2} s^{-1}). Si-release rates were slower, but similar in UPW (-9.82 ± 0.03), 0.35 mol kg^{-1} Na_2SO_4 (-9.80 ± 0.07), and 5.7 mol kg^{-1} NaCl (-9.69 ± 0.04). Therefore, Si-release rates increase with increasing Na_2SO_4 concentration, but decrease with increasing NaCl concentration.

Non-stoichiometric dissolution is observed in the aqueous solutes produced in all experiments (Figs. 1 and 3). Ca:Si ratios measured in each experiment are generally greater than would be observed if the pyroxene dissolved via congruent dissolution (elements released in the stochiometric ratios observed in the starting material shown as the lines Fig. 3). However, Ca:Si ratios are similar to stoichiometric proportions in the 0.35 mol kg^{-1} NaCl experiments. Mg:Si ratios are generally similar to or lower than expected for congruent dissolution in all the solutions. Fe:Si ratios also indicate incongruent dissolution in all experiments, producing ratios lower than expected for congruent dissolution in all the experiments except samples from the 5.7 mol kg^{-1} NaCl, where Fe:Si ratios are greater than expected for stoichiometric dissolution (Fig. 3C).

3.2. Microscopy-based comparative qualitative dissolution rates in high salinity brines

Unreacted diopside surfaces were examined for comparison with reaction products. While some fines are present on the initial diopside surfaces, the surfaces appear largely unaltered (Fig. 4A; see also additional images in Phillips-Lander et al., 2017). In general, qualitative assessments show that diopside dissolved forming etch pits and denticles along edges in each of the solutions tested (Table 2; Fig. 4). Significant clay formation on the pyroxene surface is also observed in each solution. Notably, clay minerals and denticles were also observed in both the 2 mol kg^{-1} $NaClO_4$ and 9 mol kg^{-1} $CaCl_2$ brine experiments (Fig. 4B1). Clay minerals observed in SEM largely demonstrated the "cornflake" texture (Fig. 4) noted in previous studies of clay minerals on pyroxene surfaces (Velbel and Barker, 2008 and references therein).

In UPW experiments ($aH_2O = 1$), incipient etch pits lined with nanoscale denticles are observed (Fig. 4C2). Curved platelet-shaped features are observed on the diopside surface in some places (Fig. 4C1). Clay mineral coverage of the diopside surface is estimated to be approximately 10% based on SEM analysis (Table 2). Similar dissolution textures are also observed on diopside surfaces reacted with 0.35 mol kg^{-1} Na_2SO_4 ($aH_2O = 0.98$) brine. Etch pits formed in 0.35 mol kg^{-1} Na_2SO_4 are more common than in UPW but remain small in scale and are lined with incipient denticles measuring less than 1 μm in length (Fig. 4; Phillips-Lander et al., 2017). Clay coverage remains minimal (~20%) in dilute sulfate solutions. In contrast, the greatest degree of dissolution is observed in 0.35 mol kg^{-1} NaCl ($aH_2O = 0.99$) solution, where large portions of the diopside surface are covered in etch pits and denticles (Fig. 4D1-2). However, the percent of clay coverage (~20%) mirrors other experimental solutions with high activities of water (Table 2).

The extent of dissolution textures increased in concentrated 2.5 mol kg^{-1} Na_2SO_4 brine ($aH_2O = 0.95$) relative to dilute (0.35 mol kg^{-1}) Na_2SO_4 (Fig. 4G). Clay minerals cover roughly 40% of the observed diopside surfaces in the concentrated 2.5 mol kg^{-1} Na_2SO_4 brine (Table 2). Fewer etch pits were observed in the 2.5 mol kg^{-1} Na_2SO_4 samples, but they were larger and more well-developed with generally longer denticle lengths (Fig. 4G) than those observed in the 0.35 mol kg^{-1} Na_2SO_4 (Fig. 4E). Similar dissolution etch pit sizes and densities were observed on diopside minerals weathered in 2 mol kg^{-1} $NaClO_4$ ($aH_2O = 0.9$) (Fig. 4B) and 0.35 mol kg^{-1} Na_2SO_4 (Fig. 4E). Approximately half of observed surfaces reacted

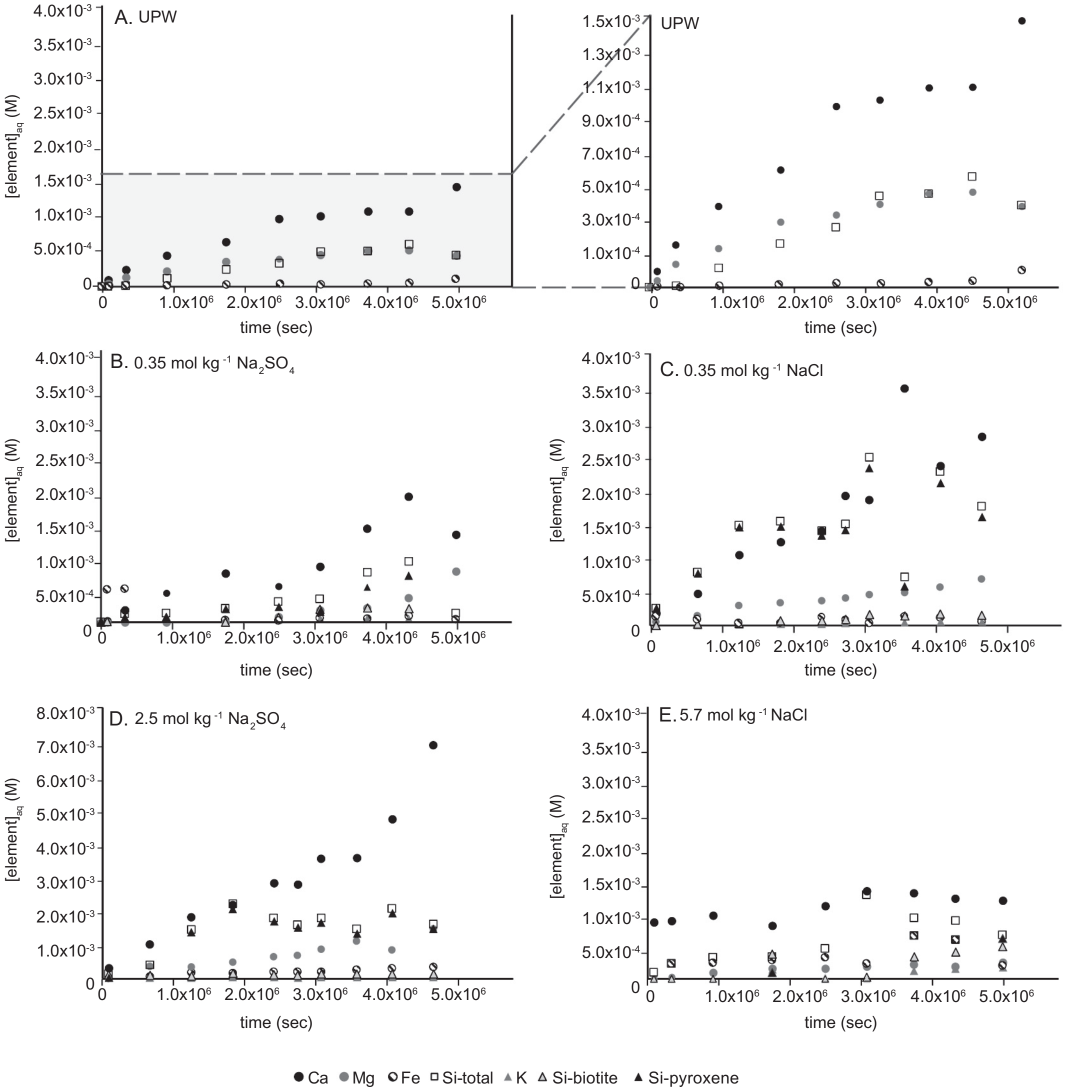

Fig. 1. Representative aqueous data for each experimental trial, including Ca (black circles), Mg (dark grey circles), Fe (striped with black outlines), Si-total (white squares with black outlines) K (dark grey triangles), and Si-biotite (light grey triangles with black outlines), and Si-pyroxene (black triangles). (A) UPW, (B) 0.35 mol kg^{-1} Na_2SO_4, (C) 0.35 mol kg^{-1} NaCl, (D) 2.5 mol kg^{-1} Na_2SO_4, and (E) 5.7 mol kg^{-1} NaCl. $CaCl_2$ aqueous data were below detection limits; aqueous data were not collected for $NaClO_4$ experiments.

with 2 mol kg^{-1} $NaClO_4$ were covered in clay minerals (Table 2). Etch pit densities decreased in 5.7 M NaCl ($aH_2O = 0.75$); however well-developed denticles were observed (Fig. 4F). In addition, clay minerals cover approximately 40% of observed mineral surfaces and in places SiO_2 spherules are also observed (Fig. 4F). Small (<1 µm) etch pits, lined with denticles are observed on the surface of pyroxene weathered in 9 mol kg^{-1} $CaCl_2$ ($aH_2O = 0.35$) (Fig. 4H). In $CaCl_2$ brines, diopside surfaces appear to be converted to clay minerals in some places, leading to ~40% of observed surfaces covered in clay minerals (Table 2).

3.3. Reaction products

Both SEM and XRD analyses indicate the presence of clay minerals in brine weathering experiments. In general, SEM analysis indicates the amount of mineral surface covered by clay minerals increased in higher salinity NaCl and Na_2SO_4 solutions (Fig. 4; Table 2). XRD analysis of UPW experiment reaction products indicated only the presence of diopside and biotite (<1%), which suggests clay minerals observed in SEM were too low in concentration to be detected with bulk powder XRD or represent altered biotite edges (Fig. 5). Indeed, EDXA analysis of apparent clay minerals observed in UPW experiments yielded chemistries consistent with altered biotite (Fig. 6, Supplemental Table 2), with Fe/Mg depleted relative to other cations and potential Al-enrichment of the altered biotite.

Diopside chips from the 2 mol kg^{-1} $NaClO_4$ experiments were analyzed with SEM, but we did not have enough material for XRD analysis. We observed that clay minerals covered approximately half of the diopside surface reacted with 2 mol kg^{-1} $NaClO_4$ based on SEM analysis. EDXA analyses of these reaction products displayed a compositional trend between altered biotite and Fe-Mg-

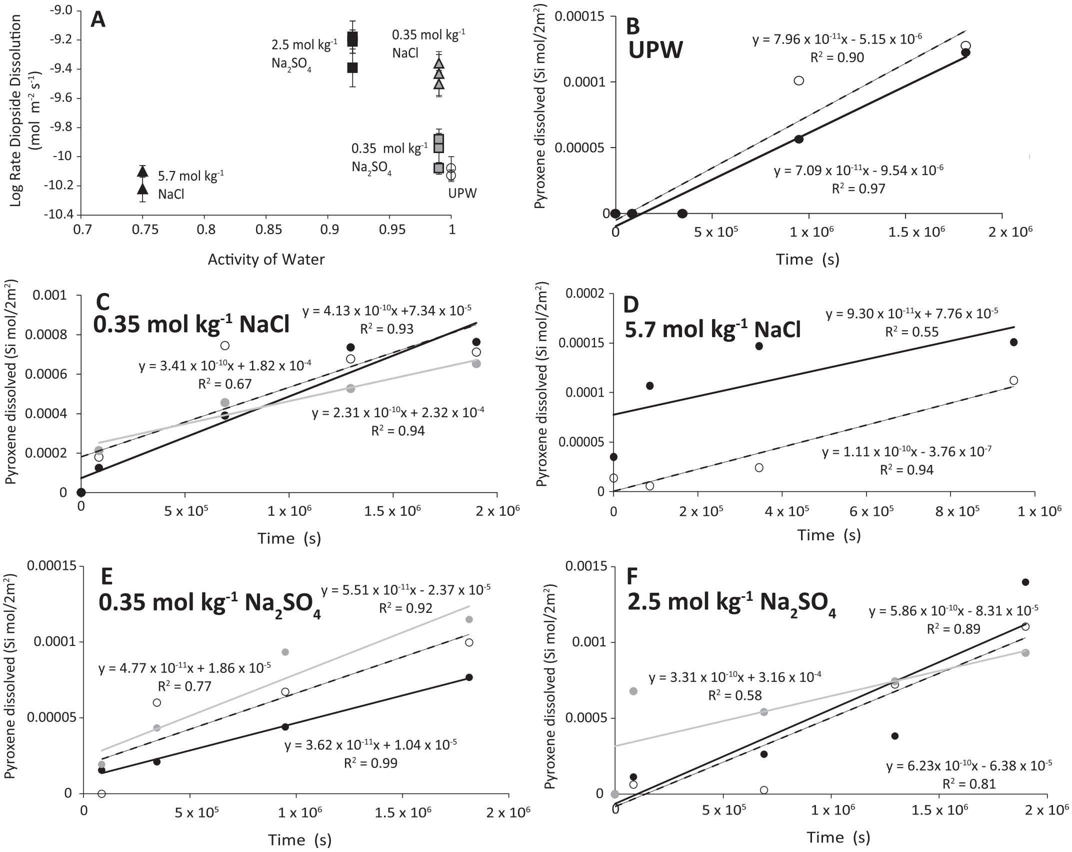

Fig. 2. Summary of Si-based pyroxene dissolution rates. (A) Log pyroxene dissolution rates as a function water activity. Circles represent UPW rates, triangles represent NaCl rates, and squares represent Na_2SO_4 rates. (B–F) Pyroxene dissolution rates determined based on a linear fit (grey, black and dashed lines for each replicate) of the Si released to solution (grey, black, and white circles, representing each replicate) during the first 2 million seconds (~23 days) in ultrapure water (B), 0.35 mol kg^{-1} NaCl (C), 5.7 mol kg^{-1} NaCl (D), 0.35 mol kg^{-1} Na_2SO_4 (E), and 2.5 mol kg^{-1} Na_2SO_4 (F). Uncertainties in the individual measurements are smaller than the size of the symbol.

rich clay mineral chemistries also observed in the other brine weathering experiments, with increasing Fe-enrichment relative to other cations (Fig. 6).

No secondary reaction products or biotite were observed with XRD in 0.35 mol kg^{-1} Na_2SO_4 brines (Fig. 5). However, SEM analyses demonstrated the presence of both clay minerals and biotite (Fig. 4). Some of these clay minerals follow the general Fe/Mg-enrichment trend observed in the other brine weathering experiments in this study, but two points lie near the biotite composition (Klein and Hurlbut, 1985) which suggest some areas of biotite remain (Fig. 6). In 2.5 mol kg^{-1} Na_2SO_4 brine secondary clay minerals were detected with XRD, based on a major peak at 12.34 Å (Fig. 5). SEM with EDXA analyses of Na_2SO_4 brine samples demonstrate these clay minerals follow the enrichment trend in Fe/Mg observed in other brine experiments.

Secondary clay minerals were also detected with XRD in both 0.35 mol kg^{-1} and 5.7 mol kg^{-1} NaCl brines, based on a major peak at 14.94 Å, which suggests the presence of vermiculite (Fig. 5). SEM with EDXA of the NaCl brine weathering products indicate clay minerals associated with pyroxene dissolution are Fe-rich, which supports aqueous data which shows relatively little iron in solution in the 0.35 mol kg^{-1} NaCl experiments. This suggests Fe-rich reaction products formed during dissolution in the dilute NaCl solution (Fig. 6, Supplemental Table 2). Clay minerals were detected in 9 mol kg^{-1} $CaCl_2$ brines using SEM and EDXA, however, no secondary phases were detected in 9 mol kg^{-1} $CaCl_2$ reaction products with XRD. Clay minerals observed via SEM in the 9 mol kg^{-1} $CaCl_2$ experiments are compositionally similar to those formed under other brine weathering conditions, with high Fe-Mg concentrations (Fig. 6, Supplemental Table 2). EDXA data indicate the clay minerals observed are generally Al-poor (1–3 wt%), suggesting the majority of clays are derived from diopside dissolution. There are a few clays with Al contents of 5–10 wt%, however, they are the minority (Supplemental Table 2).

4. DISCUSSION

Our study is the first to examine the effect of circumneutral, high salinity brines on pyroxene mineral dissolution rates and directly compare these results with more dilute solutions. Based on the aqueous solute data, incongruent dissolution was observed in all of the experiments and significant secondary precipitation of clays and silica

Table 1
Diopside dissolution rates (mol m^{-2} s^{-1}).

T (°C)	pH	aH_2O	Solution	Log rate Si release (mol Si m^{-2} s^{-1})	Source
298	–	0.35	9 mol kg^{-1} $CaCl_2$	–	This study
298	–	0.35	9 mol kg^{-1} $CaCl_2$	–	This study
298	–	0.35	9 mol kg^{-1} $CaCl_2$	–	This study
298	6.2	0.75	5.7 mol kg^{-1} NaCl	-9.82 ± 0.14	This study
298	6.2	0.75	5.7 mol kg^{-1} NaCl	-9.94 ± 0.09	This study
298	6.2	0.92	2.5 mol kg^{-1} Na_2SO_4	-8.90 ± 0.11	This study
298	7.1	0.92	2.5 mol kg^{-1} Na_2SO_4	-9.11 ± 0.13	This study
298	6.2	0.92	2.5 mol kg^{-1} Na_2SO_4	-8.93 ± 0.08	This study
298	5.5	0.99	0.35 mol kg^{-1} Na_2SO_4	-9.80 ± 0.04	This study
298	5.5	0.99	0.35 mol kg^{-1} Na_2SO_4	-9.67 ± 0.10	This study
298	5.5	0.99	0.35 mol kg^{-1} Na_2SO_4	-9.60 ± 0.07	This study
298	5.2	0.99	0.35 mol kg^{-1} NaCl	-9.08 ± 0.06	This Study
298	5.2	0.99	0.35 mol kg^{-1} NaCl	-9.15 ± 0.15	This study
298	5.2	0.99	0.35 mol kg^{-1} NaCl	-9.22 ± 0.09	This study
298	6.5	1.00	UPW	-9.85 ± 0.04	This study
298	6.6	1.00	UPW	-9.80 ± 0.08	This study
298	6.0	1.00	phthalate	−10.83	Knauss et al. (1993)
298	6.5	1.00	NaOH	−10.99	Golubev et al. (2005)
298	7.7	1.00	$NaOH + Na_2CO_3$	−11.03	Golubev et al. (2005)
298	8.0	1.00	KOH	−10.97	Knauss et al. (1993)
298	8.0	1.00	$NaOH + Na_2CO_3$	−11.00	Golubev et al. (2005)
298	8.3	1.00	$NaOH + Na_2CO_3$	−11.02	Golubev et al. (2005)
298	8.5	1.00	$NaOH + Na_2CO_3$	−11.03	Golubev et al. (2005)
298	8.6	1.00	NaOH	−11.10	Golubev et al. (2005)
298	8.7	1.00	$NaOH + Na_2CO_3$	−11.09	Golubev et al. (2005)
298	5.5	1.00	HCl	−10.86	Golubev et al. (2005)
298	5.3	1.00	HCl	−11.03	Golubev et al. (2005)

spherules were also observed. Cation:Si ratios (Fig. 3) and the presence of secondary clay minerals indicate pyroxenes dissolve incongruently; therefore, the Si-based rates represent minimum dissolution rates. Despite the precipitation of secondary phases, Si-based dissolution rates observed in all of the experiments are slightly faster than Si-based diopside dissolution rates observed in other studies at similar pH and temperature conditions (Table 1). However, dissolution rates are difficult to directly compare between different laboratories to due to different experimental methods but can be compared within a single laboratory with the same experimental conditions (Arvidson et al., 2003).

Previous studies of mineral dissolution in brines indicate sulfate, silicate, and clay mineral dissolution rates often decrease with decreasing activity of water and higher salt concentrations (Elwood Madden et al., 2017; Miller et al., 2016; Steiner et al., 2016; Olsen et al., 2015; Pritchett et al., 2012). However, the minimum Si-based dissolution rates combined with SEM images of reacted grains collected in this study suggest that pyroxene dissolution rates increase as the concentration of Na_2SO_4 increases, despite significantly lower water activities. Based on the SEM images, significant pyroxene dissolution also occurred in high salinity NaCl, $CaCl_2$, and $NaClO_4$ solutions. Therefore, this study demonstrates that pyroxene dissolution at circum-neutral pH is dependent on both solution chemistry and activity of water. Similar effects have also been observed in previous studies of quartz and carbonate mineral dissolution at circum-neutral pH that indicate both cations and anions present in solution, as well as water activity influence mineral dissolution rates and rate trends (e.g., Phillips-Lander et al., 2018; Ruiz-Agudo et al., 2009; Gledhill and Morse, 2006; Arvidson et al., 2006; Dove, 1999; Dove and Nix, 1997).

4.1. Solution chemistry effects

The minimum diopside dissolution rates measured in UPW (-9.82 ± 0.03 log mol m^{-2} s^{-1}) based on Si-release rates in this study are similar to dissolution rates observed in 5.7 mol kg^{-1} NaCl and 0.35 mol kg^{-1} Na_2SO_4 but are significantly slower than the minimum dissolution rates observed in both 0.35 mol kg^{-1} NaCl and 2.5 mol kg^{-1} Na_2SO_4 solutions. In addition, significant pyroxene dissolution and clay formation was also observed in SEM images of 9 mol kg^{-1} $CaCl_2$ and 2 mol kg^{-1} $NaClO_4$ experiments. Therefore, background electrolytes have a significant effect on diopside dissolution rates. The effects of solution chemistry are well-documented for Si-release from quartz and amorphous SiO_2 (Dove, 1999); however, diopside contains Ca, Mg, and Fe cations as well. Therefore, the formation of aqueous Ca-Mg-Fe-SO_4-Cl complexes and changes in redox conditions (in the case of Fe) may also influence cation-based diopside dissolution rates (Hoch et al., 1996). In our experiments, we observed that the addition of sulfate to solution increases $Ca_{(aq)}$ release from diopside relative to UPW (Figs. 1 and 3). Indeed, the highest $Ca_{(aq)}$:$Si_{(aq)}$ ratios are observed in the sulfate brines (Fig. 3). We suggest diopside dissolution rates increase in sulfate brines due to Ca-SO_4 complex formation ($\log K_{Ca\text{-}SO4} = 2.23$;

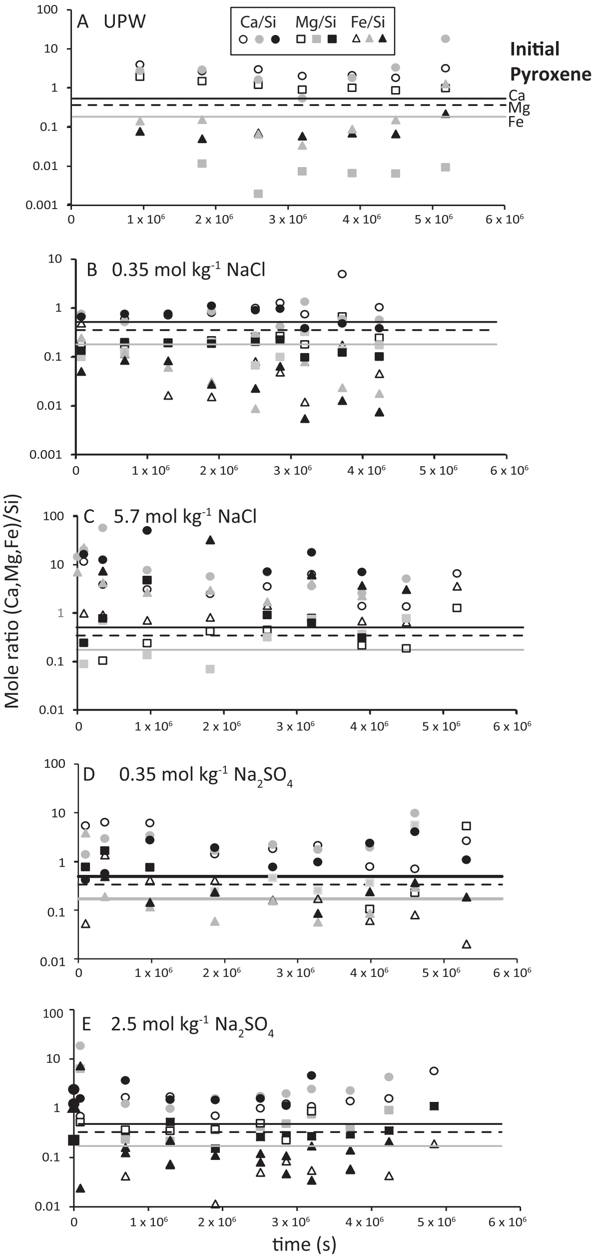

Fig. 3. Ratios of cations released to solution indicate diopside dissolution are incongruent in all experimental solutions. Ca is preferentially released in all the experiments, while Fe/Si ratios are less than would be expected in all the experiments except the 5.7 mol kg^{-1} NaCl solution (C) where both Ca and Fe are preferentially released compared to Si. Mg is preferentially released relative to Si in the UPW experiments (A), while near-stochiometric ratios are observed in the other solutions. These patterns likely reflect both preferential leaching and precipitation of secondary minerals following dissolution.

Högfeldt, 1982). Mg-mobilization is also higher in sulfate brines relative to chloride brines and UPW, likely due to the formation of Mg-SO_4 complexes ($\log K_{Mg\text{-}SO4} = 2.43$; Högfeldt, 1982), resulting in preferential Mg release in sulfate solutions as well. Similar increases in Ca- and Mg- carbonate dissolution rates in Na_2SO_4 brines at circum-neutral pH have been also been attributed to the combined influence of water-exchange rates at the mineral surface and Ca-SO_4 or Mg-SO_4 complex formation (Phillips-Lander et al., 2018; Ruiz-Agudo et al., 2009). In contrast, decreasing Ca- and Mg-based dissolution rates observed in solutions with higher NaCl concentrations are likely due to the decreasing activity of water in higher concentration chloride brines, as H_2O may be more effective at complexing Ca and Mg compared to Cl^- in chloride solutions when sulfate is absent.

Our experiments also indicate Si-based dissolution rates increase in sulfate brines with increasing salinity and decreasing activity of water. While Si-based dissolution rates also increase in dilute NaCl solutions, Si-release rates in the near-saturated NaCl brine are similar to those observed in the UPW experiments. These results suggest Na^+ ions in solution likely increase Si-release rates as has been documented in several previous studies of silicate dissolution (Tanaka and Takahashi, 2005; Icenhower and Dove, 2000; Dove, 1999), but this effect is offset by decreased water activity. Increased quartz dissolution rates in the presence of Na^+ have attributed to the formation of Na-SiO_3 complexes in NaCl solutions ranging from 0.001 to 1 M, which is significantly more dilute than our near-saturated 5.7 mol kg^{-1} NaCl brine (e.g. Karlsson et al., 2001; Icenhower and Dove, 2000; Dove, 1999; Dove and Nix, 1997; Dove and Elston, 1992). Dove (1999) also demonstrated cations, particularly Na and Ca, increase Si-mobilization from silica glass, but Mg reduces the Si-mobilization rate. In our solutions, all of the cations released via diopside dissolution (Ca, Mg, and Fe) are significantly lower in concentration than Na; therefore, Ca, Mg, and Fe likely have little influence compared to Na in our experiments. Based on these experiments and previous studies. our results suggest Na-brines also increase diopside dissolution rates.

Similar apparent Si-based dissolution rates in the 5.7 mol kg^{-1} NaCl experiments and UPW experiments are likely due to precipitation of secondary silicate phases, including both smectites detected in XRD and SEM and SiO_2 spherules detected in SEM. Tanaka and Takahashi (2005) demonstrated aqueous silica concentrations are different in solutions containing > 0.5 M Na depending on whether the counter ion present is Cl^- or SO_4^{2-}. Silica concentrations decreased in the chloride solutions due to silica polymerization and the formation of cyclic silicate complexes which "salt out" of solution (Tanaka and Takahashi, 2005). In contrast, aqueous silica concentrations increased in higher salinity sulfate solutions, likely due to partial hydrolysis of the sulfate ion, which produces OH^- ligands that further solubilize silica (Tanaka and Takahashi, 2005). A similar "salting out" process may occur in our 5.7 mol kg^{-1} NaCl brine experiments, where measured $Si_{(aq)}$ concentrations are highly variable (Fig. 3) and we observe precipitation of SiO_2 spherules on dissolved diopside surfaces with SEM (Fig. 4F.1). Hence, the aqueous Si variability we observe in the high concentration NaCl brine experiments may be due to precipitation of these secondary SiO_2 spherules and clay minerals, which complicates rate measurements. Based on the textures observed

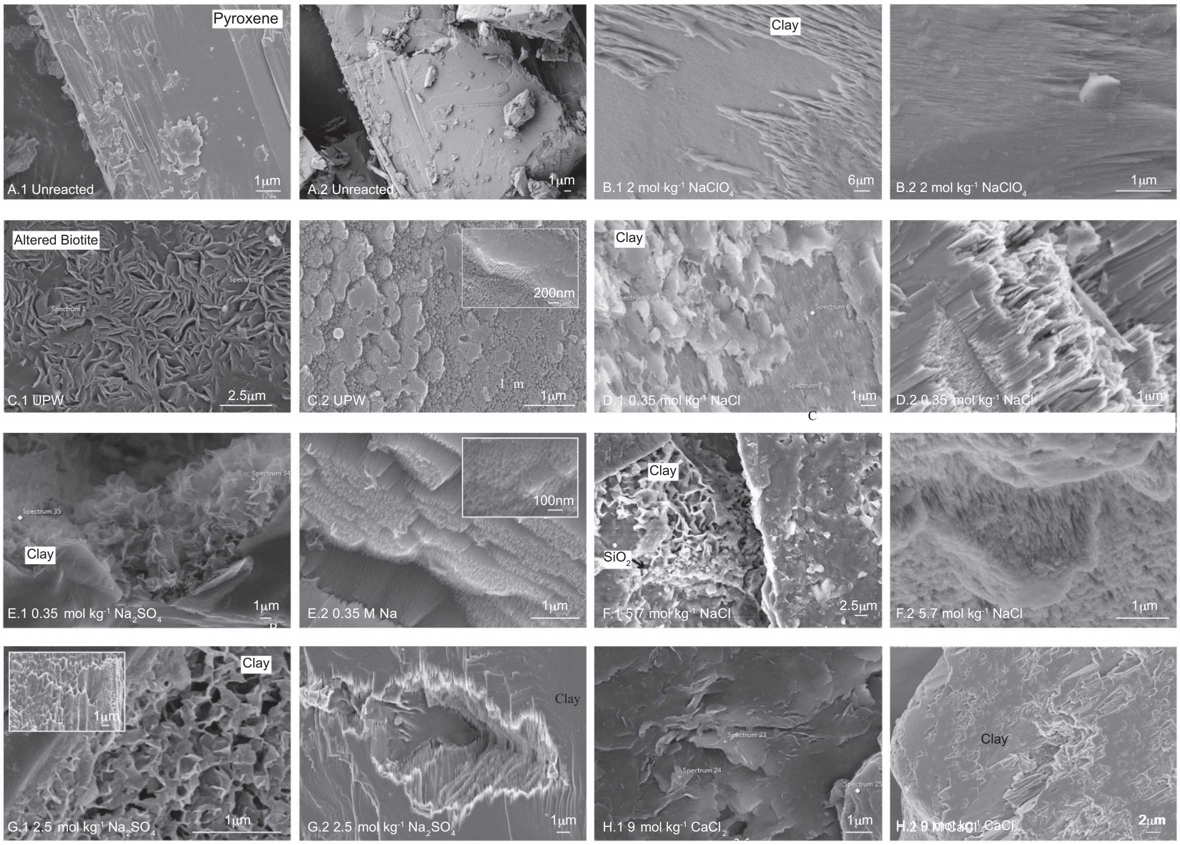

Fig. 4. Comparison of unreacted pyroxene chips (A.1 and A.2) with pyroxene chips weathered in UPW (C.1 and C.2) and brines including (B) 2 mol kg^{-1} $NaClO_4$, (D) 0.35 mol kg^{-1} NaCl, (E) 0.35 mol kg^{-1} Na_2SO_4, (F) 5.7 mol kg^{-1} NaCl, (G) 2.5 mol kg^{-1} Na_2SO_4, and (H) 9 mol kg^{-1} $CaCl_2$. Pyroxene weathering in perchlorate results in the formation of some clay and altered biotite (B.1) and dissolution of the pyroxene surface (B.2) The greatest degree of dissolution was observed in 0.35 mol kg^{-1} NaCl, where clay minerals cover weathered pyroxene surfaces in some areas (D.1) and most pyroxene surfaces are display significant dissolution and denticle formation (D.2). Altered biotite was observed in UPW (C.1), which supports XRD data. Both (C.2) UPW and (E) 0.35 mol kg^{-1} Na_2SO_4 appears less dissolved than 0.35 mol kg^{-1} NaCl, which supports aqueous rate determinations. The scale of denticles for B.2 and E.2 are shown in the inset images. Concentrated (2.5 mol kg^{-1}) Na_2SO_4 appears more weathered than (C) UPW and (E) 0.35 mol kg^{-1} Na_2SO_4, which also supports our rate data. Clay minerals are common in etch pits (G.1). These pits are common on some surfaces (G.2); however, on other surfaces denticles appear to be transforming to clay in situ (G.1 inset). Large denticles, comprised of smaller denticles typify dissolution in 5.7 mol kg^{-1} NaCl (F.2). Both clay minerals and SiO_2 spherules are detected in 5.7 mol kg^{-1} NaCl, which may explain the differences in $Si_{(aq)}$ between experimental trials (F.1). Minimal dissolution was observed in 9 mol kg^{-1} $CaCl_2$, including few etch pits on mineral surfaces (H.2) and alteration of the pyroxene surface to clay (H.1). Together these data suggest aH_2O does not solely control pyroxene dissolution.

Table 2
Qualitative assessment of diopside weathering.

Condition	aH_2O	Etch pits	Denticles	Clay coverage
UPW	1.00	++	++	10%
0.35 mol kg^{-1} NaCl	0.99	+++	+++	20%
0.35 mol kg^{-1} Na_2SO_4	0.98	+++	++	20%
2.5 mol kg^{-1} Na_2SO_4	0.95	++	++	40%
2 mol kg^{-1} $NaClO_4$	0.90	++	++	50%
5.7 mol kg^{-1} NaCl	0.75	+	++	40%
9 mol kg^{-1} $CaCl_2$	0.35	+	+	40%

in these high concentration NaCl experiments, including some etch pits with moderate denticle formation and moderate-high clay coverage (Table 2), dissolution likely occurs at rates similar to those observed in the 0.35 mol kg^{-1} NaCl solution. In addition, the precipitation of SiO_2 spherules in these experiments may provide an additional mechanism for explaining Si-rich coatings observed on some rocks on Mars (Kraft et al., 2003; Milliken

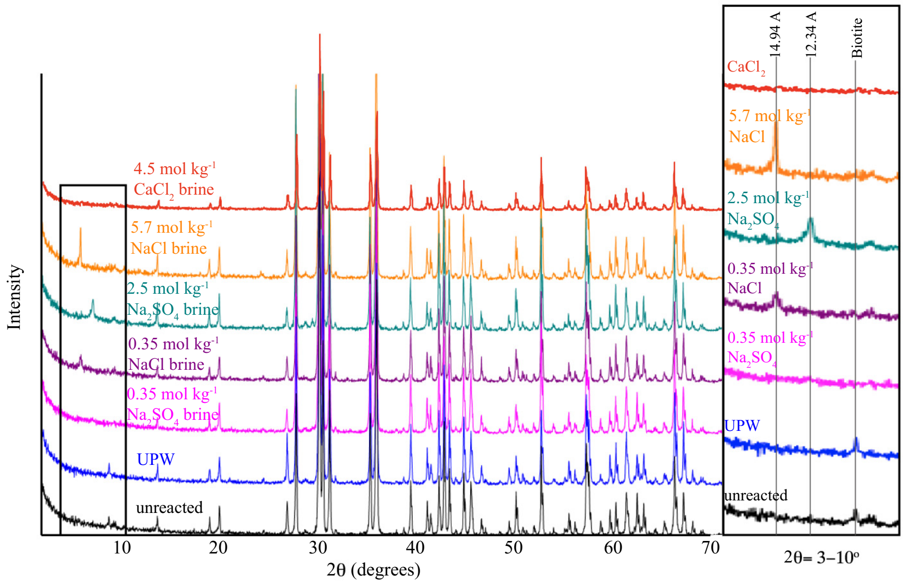

Fig. 5. XRD patterns for each experimental trial. The unreacted sample are primarily pyroxene contains ~ 1% biotite (black line). UPW experiments indicate the presence of pyroxene and ~ 5% biotite (blue line). Chloride brines indicate the presence of pyroxene and a 14.94 Å clay mineral (red and yellow lines). The 0.35 mol kg^{-1} Na_2SO_4 experiment contains only pyroxene, while the 2.5 mol kg^{-1} sulfate brine also contains a 12.34 Å clay. (For interpretation of the references to colour in this figure legend, the reader is referred to the web version of this article.)

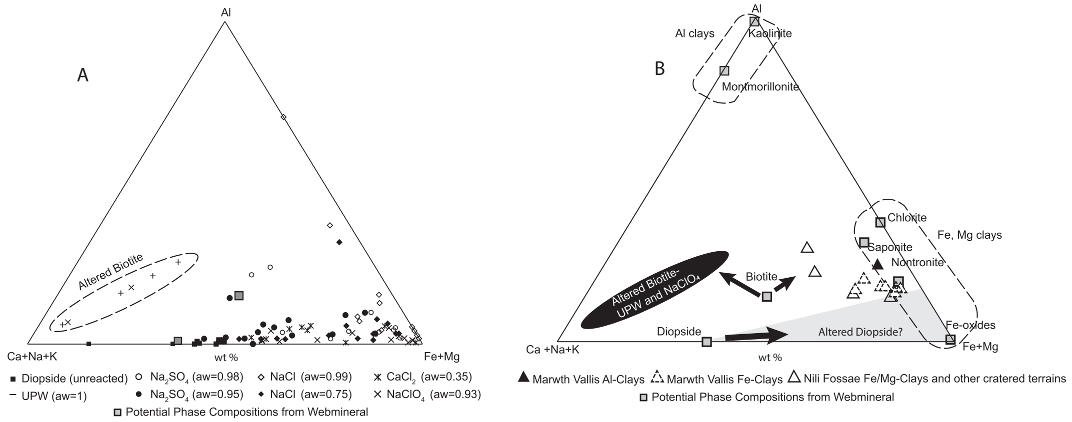

Fig. 6. (A) Ternary plot of wt% Ca + Na + K, Fe + Mg, and Al based on EDS data collected in conjunction with SEM analysis indicates most experiments track along a continuum line between diopside and clay minerals, with an enrichment in Fe and Mg relative to Ca. B) Clay minerals observed on Mars (Ehlmann et al., 2011) are also Fe/Mg rich, and fall between the potential diopside and biotite weathering trends in terms of Al content.

et al., 2008; Squyres et al., 2008). Therefore, at circumneutral pH, the effects of electrolytes on diopside dissolution are pronounced.

Fe:Si ratios observed in the 5.7 mol kg^{-1} NaCl experiments are approximately one order of magnitude greater than in any of the other experiments. This stark increase in Fe-release in the near-saturated NaCl experiments may be linked to both the formation of Fe-Cl complexes and/or the decreased Fe oxidation in high salinity chloride brines. Variations in observed Fe concentration could also be due to variations in iron(hydr)oxide colloid particle sizes, as smaller (<0.2 μm) secondary precipitates could pass through the filter and subsequently dissolve due to acidification, while larger colloids would be trapped on the filter. Pritchett et al., (2012) also observed increased Fe-mobilization during jarosite dissolution in 5.7 mol kg^{-1} NaCl and 9 mol kg^{-1} $CaCl_2$ brines, which they attributed to Fe complexation by the chloride ion. Similar results were recently observed in siderite ($FeCO_3$) dissolution experiments as well, where faster dissolution rates were observed in high salinity 3 mol kg^{-1} $MgCl_2$ ($aH_2O = 0.73$) than in 1.9 mol kg^{-1} $MgSO_4$ ($aH_2O = 0.95$) brines (Cullen et al., 2017). Iron oxide minerals also dissolve faster in chloride brines compared to perchlorate solutions (Sidhu et al., 1981), suggesting strong Fe-Cl complexation. Indeed, we and many other geochemists commonly rely on Fe-Cl complex-driven dissolution when we use HCl to clean our iron-oxide-stained glass and plastic ware. However, Millero et al., (1995) found that $FeCl^{2+}$ (log $K = 0.57$) and $FeCl_2^+$ (0.13) complexes are significantly less likely to form than $FeSO_4^+$ (2.58) and $Fe(SO_4)_2^-$ (3.54) in solutions up to seawater concentrations ($I = 0.72$ M), which suggests Fe-Cl complex formation may not be the sole driver of greater Fe-mobilization rates in brines. Despite these predictions, aqueous Fe concentration data and dissolution rates observed in this and other studies (Sidhu et al., 1981; Pritchett et al., 2012) suggest Fe-Cl complexation is an important mechanism for dissolving Fe-bearing minerals.

However, decreased oxygen solubility in solutions with increasing salinity and decreasing activity of water (Geng and Duan, 2010) may also result in higher apparent Fe-release rates. Decreased oxygen solubility in the near-saturated NaCl brine could lead to higher aqueous Fe concentrations since the Fe^{2+} ions released from the diopside are less likely to oxidize to form less soluble Fe^{3+}. While similar quantities of Fe^{2+} may have been released to solution in the other solutions, it likely oxidized quickly and reprecipitated in a secondary reaction product due to higher oxidation states in the solution, resulting in slower apparent Fe-based dissolution rates and highly incongruent aqueous ion ratios.

Finally, a third possible explanation for elevated Fe:Si ratios in Cl versus sulfide brines relates to the possible role of the anion in oxidation kinetics. Fe^{2+} has been shown to oxidize more quickly in sulfate-rich solutions compared to solutions containing chloride or nitrate (Le Truong et al., 2004). Peroxide (H_2O_2) is produced during the sequence of reactions following Fe(II) oxidation by O_2; therefore the presence of sulfate in the brines may have accelerated Fe oxidation and removal through precipitation in our experiments. On the other hand, previous studies suggested chloride or sulfate had little impact on iron oxidation under conditions where H_2O_2 may also have formed (e.g., Craig et al., 2009). Since O_2 solubility also decreases in chloride brines, ferrous iron may remain in solution for longer periods of time, resulting in higher aqueous Fe concentrations since Fe^{2+} is significantly more soluble than Fe^{3+} (Morgan and Lahav, 2007). Therefore, the combination of increased chloride complexation, decreased O_2 solubility, and slower oxidation rates in the 5.7 mol kg^{-1} NaCl brine likely contributes to the increase in aqueous Fe:Si observed in these experiments. This suggests redox processes also play a role in Fe-mobilization in high salinity brines. However, the effects of chloride complexation, O_2 solubility, and oxidation kinetics cannot be fully disentangled based on these experiments. Experiments directly comparing dissolution rates in chloride brines with varying levels of O_2 would be required to determine the independent roles of $O_{2(aq)}$ and chloride complexation in high salinity brines.

4.1.1. *Activity of water influences aqueous dissolution rates*

Based on our results, solution cation and anion chemistry clearly influence diopside dissolution at circumneutral pH. Water activity likely also plays a role, however, the effects of varying activity of water are more difficult to discern from these experiments. Very slow diopside dissolution was observed in the lowest water activity experiments (9 mol kg^{-1} $CaCl_2$ brines, $aH_2O = 0.35$), as cations were below detection limits and SEM analysis revealed little evidence of diopside weathering (Fig. 4). Conversely, the near-saturated 5.7 mol kg^{-1} NaCl brine ($aH_2O = 0.75$), UPW ($aH_2O = 1$), and 0.35 mol kg^{-1} Na_2SO_4 ($aH_2O = 0.99$) all have similar Si-based dissolution rates. In addition, Si spherules observed in SEM images from the 5.7 mol kg^{-1} NaCl dissolution products suggest Si likely precipitated from solution, thus lowering the observed dissolution rate. Therefore, pyroxene likely dissolved faster in both the near-saturated 5.7 mol kg^{-1} NaCl ($aH_2O = 0.75$) and 2.5 mol kg^{-1} Na_2SO_4 ($aH_2O = 0.9$) brines than in UPW. Overall, these observations demonstrate that activity of water does not strongly influence diopside dissolution rates in near-neutral solutions until solutions reach extremely low values of water activity (<0.75); instead, ion chemistry and/or O_2 solubility have stronger effects on dissolution rates. In particular, the varying effects of Cl^- and SO_4^{2-} on Ca, Mg, and Fe released from the diopside structure underscore the role of specific ion-ligand interactions in moving atoms from the mineral surface to solution. The slow rate of diopside dissolution in 9 mol kg^{-1} $CaCl_2$ may also be due to the common ion-effect with Ca in both the mineral and abundantly in solution. This suggests water molecules act as relatively weak ligands in facilitating diopside dissolution in near neutral solutions compared to chloride and sulfate complexes.

4.2. Pyroxene dissolution textures reflect dissolution rates

Previous textural studies of pyroxene dissolution have focused primarily on quantitative textural analyses (Phillips-Lander et al., 2017; Velbel and Losiak, 2010; Velbel, 2007; Schaetzl et al., 2006; Mikesell et al., 2004; Hall and Horn, 1993; Argast, 1991; Hall and Michaud, 1988), including statistical analyses of measurements of the apparent apical angle and length of denticles, tooth-like structures formed on the margins of etch pits. In a meta-analysis of previously measured apparent angles, Velbel and Losiak (2010) noted these quantitative measures of weathering textures do not vary systematically with mineral composition. Phillips-Lander et al., (2017) extended this work to show denticle apical angle also does not vary systematically with solution chemistry; however, denticle length does generally correlate with extent of aqueous alteration (i.e. reaction progress) regardless of solution conditions. While these previous quantitative assessments have focused on a fairly narrow-range of dissolution parameters, qualitative assessments of mineral weathering can include grain shape, etch pits, grooves, fractures, and clay mineral surface coverage to assess weathering (Phillips-Lander et al., 2014; Andò et al., 2012; Velbel, 2007). These weathering textures can be observed at a variety of scales from sub-micron to cm that indicate progressive dissolution (Velbel, 2007; Andò et al., 2012).

Our qualitative assessment of pyroxene dissolution textures supports our aqueous dissolution rates, suggesting the extent of diopside weathering and reaction products follows the following progression from least to most weathered: 9 mol kg^{-1} $CaCl_2$ < 5.7 mol kg^{-1} NaCl < UPW ≈ 2 mol kg^{-1} $NaClO_4$ ≈ 2.5 mol kg^{-1} Na_2SO_4 < 0.35 mol kg^{-1} Na_2SO_4 < 0.35 mol kg^{-1} NaCl. These relative comparisons in qualitative weathering textures generally follow the same relative relationships observed in the dissolution rate data (when available), with the exception of the 2.5 mol kg^{-1} Na_2SO_4 experiments which showed the fastest Si-based dissolution rates. Therefore, we can infer relative minimum diopside dissolution rates in the 9 mol kg^{-1} $CaCl_2$ and 2 mol kg^{-1} $NaClO_4$ based on these qualitative assessments of weathering textures. Based on the textural observations, we predict diopside dissolves relatively slowly in near-saturated $CaCl_2$ brines, likely due to a combination of both low activity of water (~0.35) and high Ca activity which inhibits release of Ca and other cations into solution from the diopside surface. Likewise, we infer diopside dissolution rates are moderate in $NaClO_4$ brines, comparable to rates observed in UPW and dilute Na_2SO_4, based on moderate etch pit and denticle formation combined with significant clay mineral coverage. Our qualitative data indicate minor dissolution and secondary clay formation occurs in perchlorate brines, on par with UPW. This supports interpretations that perchlorate essentially acts as an inert ion in solution (Gowda et al., 1984) and that aH_2O governs pyroxene dissolution in perchlorate brines. Phillips-Lander et al. (2017) indicated perchlorate may enhance denticle lengths, which could mislead estimates of the duration of aqueous alteration on Mars and in martian meteorites. However, when these data are placed in a broader qualitative context that accounts for dissolution textures and formation of secondary clay minerals, it becomes clear dissolution rates in perchlorate are slow.

4.3. Pyroxene weathering products in chloride and sulfate brines

Both limited pyroxene and biotite alteration occurred in UPW, as no clays were observed in XRD in addition to the biotite; biotite was also evident in the SEM and EDS data (Figs. 5 and 6). However, more rapid aqueous alteration in sulfate, chloride, and perchlorate brines resulted in clay minerals forming on the diopside surface during dissolution (Figs. 4 and 5; Velbel and Barker, 2008). Likely, these surface-associated neoformed clays were not detected by XRD. The variation in d-spacing and sharpness of peak profiles of the clay minerals observed in the XRD analyses of the chloride and sulfate brine experiments can be explained by progressive alteration of biotite. The ~15 Å d-spacings are consistent with complete conversion to vermiculite, while the ~ 12.3 Å spacing seen in the more concentrated brine matches expectations for hydrobiotite, a mixed-layer vermiculite-biotite that forms through progressive biotite alteration (e.g., Brindley et al., 1983). Peak height increases with increasing alteration generally follow expected trends for the expected increase in X-ray scattering from a similar number of biotite and vermiculite 2:1 phyllosilicate layers.

While clay mineral d-spacing varies between chloride and sulfate brines (Fig. 5), clay mineral chemistry is generally similar in all the experimental conditions (except UPW), suggesting clay mineral composition is not diagnostic of solution chemistry or activity of water. Biotite alteration may also be observed, particularly in the UPW and $NaClO_4$ experiments, where biotite appears to have lost Fe/Mg. Additional measurements with significantly elevated Al may also be the products of biotite alteration in NaCl and $NaSO_4$ brines. The series of low Al, high Fe/Mg composition analyses may represent diopside alteration, where Ca, Na, and K have been leached from the diopside and/or neoformed clays containing higher concentrations of Mg and Fe and slightly more Al precipitated on the surface (Fig. 6). Increasing pH conditions within the experiment over time may have also affected the formation of secondary clay minerals. While we did not measure pH directly in the experiments over time, reaction path modeling suggests that pH conditions likely evolved towards pH 7–9, where silica solubility begins to increase, thus facilitating neoform clay precipitation from solution. Overall, the precipitation of secondary clay minerals on diopside surfaces suggests significant diopside dissolution occurred, even in high salinity experiments with very low water activity. In addition, the increased clay coverage observed in the higher salinity experiments suggests that diopside dissolution in high salinity brines may result in "salting out" of abundant clay minerals due to the high ion concentrations in solution. As the diopside dissolves and adds ions to the already near-saturated brine, the solution quickly becomes saturated with respect to clay minerals (and potentially other mineral phases), resulting in secondary mineral precipitation.

4.4. Implications for Mars

Previous studies of mineral dissolution in high salinity brines have focused primarily on dissolution in near-saturated chloride brines, which lead to a clear correlation between dissolution rate and activity of water (Olsen et al., 2015; Steiner et al., 2016; Miller et al., 2016; Pritchett et al., 2012). More recent studies of mineral dissolution in chloride and sulfate brines (e.g. Phillips-Lander et al., 2018; Cullen et al., 2017) have demonstrated that both solution chemistry and water activity can influence carbonate dissolution rates. This study shows diopside dissolution rates are more strongly affected by ion chemistry than water activity, as Si-based dissolution rates increase with increasing Na_2SO_4 concentration, likely due to increased Na-SiO_3, Ca-SO_4, and Mg-SO_4 complexation at the mineral-solution interface. Abundant weathering textures observed in both dilute and near-saturated NaCl suggest that significant diopside dissolution also occurs in NaCl brines. Si-release rates in 9 mol kg^{-1} $CaCl_2$ brines were lower than the detection limit, suggesting activity of water may have some effect on diopside dissolution rates, but these effects are weaker than other variables until the activity of water drops below 0.75. However, high aqueous Fe concentrations observed in the 5.7 mol kg^{-1} NaCl brine experiments are likely due to Cl-complexation and/or low oxygen solubility.

Our experiments demonstrate that diopside dissolution and secondary clay precipitation are amplified in NaCl and Na_2SO_4 brines likely due to the effects of sulfate on Si-polymerization, formation of Na-SiO_3 complexes, low O_2 solubility, as well as the formation of aqueous Ca-, Mg-, and Fe- complexes with sulfate and chloride. These combined effects lead to relatively fast dissolution rates in Na_2SO_4 and NaCl solutions, even as the activity of water decreases. Therefore, the persistence of pyroxene minerals associated with alteration phases (salts and clay minerals) on the surface of Mars and in SNC meteorites indicates aqueous alteration either occurred in very low aH_2O brines (e.g. near-saturated $CaCl_2$) or was very brief. The presence of opal-A nanoparticles (Lee et al., 2015; Thomas-Keprta et al., 2000) and halite (Gooding et al., 1991) in the Nakhla meteorite may indicate weathering in high salinity chloride brines where SiO_2 may salt out even at circumneutral pH. This interpretation supports the assessment that dissolution within the Nakhla parent-rock occurred in circumneutral pH saline solutions over a geologically short time interval (Lee et al., 2015; Bridges and Schwenzer, 2012; Bridges et al., 2001).

Both pyroxene and sulfate minerals are also present in the John Klein and Cumberland drill samples in the Yellowknife Bay formation, Gale Crater (Vaniman et al., 2013). Pyroxene weathering in both chloride and sulfate brines preferentially releases calcium to solution relative to magnesium (Fig. 3), which may explain the prevalence of calcium sulfates in secondary veins observed in Gale Crater and Meridiani Planum. Sulfate minerals likely formed via diagenesis are commonly preserved as nodules along fractures in the Cumberland outcrop and occur as veins throughout Yellowknife Bay (Nachon et al., 2014). More recently, basaltic minerals have been also been detected in association with sulfate minerals in the Murray Formation, which was attributed to aqueous alteration (Rampe et al., 2017). Given the rapid pyroxene dissolution rates observed in high-salinity sulfate brines, post-depositional alteration within Gale Crater was likely limited in duration and/or restricted to areas directly associated with fractures to preserve pyroxene in the sediments. During these limited alteration events, high salinity sulfate brines interacting with Ca-bearing pyroxenes may have leached sufficient Ca from the minerals to precipitate the Ca-sulfate veins and nodules observed in the Gale Crater rocks (Hausrath et al., 2017).

More broadly, similar studies of carbonate dissolution (Phillips-Lander et al., 2018) in conjunction with this study on diopside dissolution, indicate rapid mineral dissolution occurs in circum-neutral pH sulfate brines even as activity of water decreases. These weathering reactions release cations to solution, which may precipitate as secondary sulfate or clay minerals. Therefore, the presence of sulfate minerals alone is not indicative of acidic weathering conditions on Mars. Additional lines of evidence, including the presence of minerals known to form only under acidic conditions, such as alunite and jarosite, are required to infer acid-sulfate weathering occurred in a given location. Diopside weathering in brines on Mars also has important implications for habitability because the dissolution of pyroxene could release redox-sensitive elements into solution (e.g., Fe, Mn), which are energy sources for chemolithotrophic organisms (Gomez et al., 2012).

ACKNOWLEDGEMENTS

This study was supported by a NASA Mars Fundamental Research Grant #NNX13AG75G. We gratefully acknowledge George Morgan of OU's Microprobe Laboratory and Preston Larson Sof OU's Sam Noble Microscopy Laboratory for their technical assistance. Additionally, we thank Rebecca Funderberg, Sheriee Parnell, Brittany Pritchett, and Jeffrey Westrop for their assistance in the laboratory and Nina McCollom for comments on earlier draft of this manuscript. We thank editor Jeff Catalano as well as Liz Rampe and two additional anonymous reviewers for their helpful comments which improved this manuscript.

APPENDIX A. SUPPLEMENTARY MATERIAL

Supplementary data to this article can be found online at https://doi.org/10.1016/j.gca.2019.05.006.

REFERENCES

Achilles C. N., Downs R. T., Ming D. W., Rampe E. B., Morris R. V., Treiman A. H., Morrison S. M., Blake D. F., Vaniman D. T. and Bristow T. F. (2017) Ground truth mineralogy vs. orbital observations at the Bagnold Dune Field. *J. Geophys. Rsh: Planets* **122**, 2144–2162.

Amundson R., Ewing S., Dietrich W., Sutter B., Owen J., Chadwick O., Nishiizumi K., Walvoord M. and McKay C. (2008) On the in situ aqueous alteration of soils on Mars. *Geochim. Cosmochim. Acta* **72**, 3845–3864.

Andò S., Garzanti E., Padoan M. and Limonta M. (2012) Corrosion of heavy minerals during weathering and diagenesis: a catalog for optical analysis. *Sedim. Geol.* **280**, 165–178.

Archer P. D., Franz H. B., Sutter B., Arevalo R. D., Coll P., Eigenbrode J. L., Glavin D. P., Jones J. J., Leshin L. A., Mahaffy P. R. and McAdam A. C. (2014) Abundances and implications of volatile-bearing species from evolved gas analysis of the Rocknest aeolian deposit, Gale Crater, Mars. *J. Geophys. Rsh: Planets* **119**, 237–254.

Argast S. (1991) Chlorite vermiculitization and pyroxene etching in an aeolian periglacial sand dune, Allen County, Indiana. *Clays Clay Min.* **39**, 622–633.

Arvidson R. S., Collier M., Davis K. J., Vinson M. D., Amonette J. E. and Luttge A. (2006) Magnesium inhibition of calcite dissolution kinetics. *Geochim. Cosmochim. Acta* **70**, 583–594.

Arvidson R. S., Ertan I. E., Amonette J. E. and Luttge A. (2003) Variation in calcite dis-solution rates: a fundamental problem? *Geochim. Cosmochim. Acta* **67**(9), 1623–1634.

Bandfield J. L. (2002) Global mineral distributions on Mars. *J. Geophys. Rsh: Planets* **107**(E6).

Bandfield J. L., Hamilton V. E. and Christensen P. R. (2000) A global view of Martian surface compositions from MGS-TES. *Science* **287**, 1626–1630.

Bandstra J. Z. and Brantley S. L. (2008) Surface evolution of dissolving minerals investigated with a kinetic Ising model. *Geochim. Cosmochim. Acta* **72**(11), 2587–2600.

Bibring J. P. et al. (2006) Global mineralogical and aqueous Mars history derived from OMEGA/Mars Express data. *Science* **312**, 400–404.

Bibring J. P., Langevin Y., Gendrin A., Gondet B., Poulet F., Berthé M., Soufflot A., Arvidson R., Mangold N., Mustard J. and Drossart P. (2005) Mars surface diversity as revealed by the OMEGA/Mars Express observations. *Science* **307**, 1576–1581.

Bish D. L., Blake D. F., Vaniman D. T., Chipera S. J., Morris R. V., Ming D. W., Treiman A. H., Sarrazin P., Morrison S. M., Downs and Achilles C. N. (2013) X-ray diffraction results from Mars Science Laboratory: mineralogy of Rocknest at Gale crater. *Science* **341**, 1238932.

Blake D. F., Morris R. V., Kocurek G., Morrison S. M., Downs R. T., Bish D., Ming D. W., Edgett K. S., Rubin D., Goetz W. and Madsen M. B. (2013) Curiosity at Gale crater, Mars: characterization and analysis of the Rocknest sand shadow. *Science* **341**, 1239505.

Brantley S. L. (2003) Reaction kinetics of primary rock-forming minerals under ambient conditions. *Treat. Geochem.* **5**, 605.

Brantley S. L. and Olsen A. A. (2014) Reaction kinetics of primary rock-forming minerals under ambient conditions. *Treat. Geochem.* **7**, 69–113.

Bridges J. C., Catling D. C., Saxton J. M., Swindle T. D., Lyon I. C. and Grady M. M. (2001) Alteration assemblages in Martian meteorites: Implications for near-surface processes. In *Chronology and evolution of Mars* (eds. R. Kallenbach, J. Geiss and W. K. Hartmann). Springer, Netherlands, pp. 365–392.

Bridges J. C. and Grady M. M. (2000) Evaporite mineral assemblages in the nakhlite (martian) meteorites. *EPSL* **176**, 267–279.

Bridges J. C. and Schwenzer S. P. (2012) The nakhlite hydrothermal brine on Mars. *EPSL* **359**, 117–123.

Bridges J. C. and Warren P. H. (2006) The SNC meteorites: basaltic igneous processes on Mars. *J. Geol. Soc.* **163**(2), 229–251.

Bristow T. F., Rampe E. B., Achilles C. N., Blake D. F., Chipera S. J., Craig P. and Grotzinger J. P., et al. (2018) Clay mineral diversity and abundance in sedimentary rocks of Gale crater, Mars. *Sci. Adv.* **4**(6), eaar3330.

Chen Y. and Brantley S. L. (1998) Diopside and anthophyllite dissolution at 25 and 90°C and acid pH. *Chem. Geol.* **147**, 233–248.

Christensen P. R., Anderson D. L., Chase S. C., Clancy R. T., Clark R. N., Conrath B. J., Kieffer H. H., Kuzmin R. O., Malin M. C., Pearl J. C. and Roush T. L. (1998) Results from the Mars global surveyor thermal emission spectrometer. *Science* **279**, 1692–1698.

Christensen P. R., Wyatt M. B., Glotch T. D., Rogers A. D., Anwar S., Arvidson R. E., Bandfield J. L., Blaney D. L., Budney C., Calvin W. M. and Fallacaro A. (2004) Mineralogy at Meridiani Planum from the Mini-TES experiment on the Opportunity Rover. *Science* **306**, 1733–1739.

Cotton A. (2008) Dissolution kinetics of clinoptilolite and heulandite in alkaline conditions. *Biosci. Horizons* **1**(1), 38–43.

Craig P., Shaw T., Miller P., Pellechia P. and Ferry J. (2009) Use of multiparametric techniques to quantify the effects of naturally occurring ligands on the kinetics of Fe(II) oxidation. *Environ. Sci. Technol.* **43**, 337–342.

Cullen, M.D., Phillips-Lander, C.M., Elwood Madden, M.E., 2017. Siderite dissolution kinetics in Mars-Analog Brines. Lunar and Planet. Sci. 48. Lunar Planet. Inst., Houston. #2379(abstr.).

Daval D., Hellmann R., Corvisier J., Tisserand D., Martinez I. and Guyot F. (2010) Dissolution kinetics of diopside as a function of solution saturation state: macroscopic measurements and implications for modeling of geological storage of CO_2. *Geochim. Cosmochim. Acta* **74**, 2615–2633.

Daval D., Hellmann R., Saldi G., Wirth R. and Knauss K. (2013) Linking nm-scale measurements of the anisotropy of silicate surface reactivity to macroscopic dissolution rate laws: new insights based on diopside. *Geochim. Cosmochim. Acta* **107**, 121–134.

Dove P. M. (1999) The dissolution kinetics of quartz in aqueous mixed cation solutions. *Geochim. Cosmochim. Acta* **63**, 3715–3727.

Dove P. M. and Elston S. F. (1992) Dissolution kinetics of quartz in sodium chloride solutions: analysis of existing data and a rate model for 25°C. *Geochim. Cosmochim. Acta* **56**, 4147–4156.

Dove P. M. and Nix C. J. (1997) The influence of the alkaline earth cations, magnesium, calcium, and barium on the dissolution kinetics of quartz. *Geochim. Cosmochim. Acta* **61**, 3329–3340.

Eggleston C. M., Hochella, Jr, M. F. and George P. A. (1989) Sample preparation and aging effects on the dissolution rate and surface composition of diopside. *Geochim. Cosmochim. Acta* **53**(4), 797–804.

Ehlmann B. L., Mustard J. F., Murchie S. L., Bibring J. P., Meunier A., Fraeman A. A. and Langevin Y. (2011) Subsurface water and clay mineral formation during the early history of Mars. *Nature* **479**, 53–60.

Elwood Madden M. E., Madden A. S., Rimstidt J. D., Zahrai S., Kendall M. R. and Miller M. A. (2012) Jarosite dissolution rates and nanoscale mineralogy. *Geochim. Cosmochim. Acta* **91**, 306–321.

Elwood Madden, M.E., Phillips-Lander, C.M., Miller, J.L., 2017. Albite dissolution in high salinity brines indicates limited aqueous alteration on post-Noachian Mars. Lunar and Planet. Sci. 48. Lunar Planet. Inst., Houston. #1346 (abstr.).

Floran R. J., Prinz M., Hlava P. F., Keil K., Nehru C. E. and Hinthorne J. R. (1978) The Chassigny meteorite: a cumulate dunite with hydrous amphibole-bearing melt inclusions. *Geochim. Cosmochim. Acta* **42**, 1213–1229.

Geng M. and Duan Z. (2010) Prediction of oxygen solubility in pure water and brines up to high temperatures and pressures. *Geochim. Cosmochim. Acta* **74**, 5631–5640.

Gledhill D. K. and Morse J. W. (2006) Calcite dissolution kinetics in Na–Ca–Mg–Cl brines. *Geochim. Cosmochim. Acta* **70**, 5802–5813.

Glover E. T., Faanur A. and Fianko J. R. (2010) Dissolution kinetics of stilbite at various temperatures under alkaline conditions. *West Afric. J. Appl. Ecol.* **16**(1).

Golubev S. V., Pokrovsky O. S. and Schott J. (2005) Experimental determination of the effect of dissolved CO2 on the dissolution kinetics of Mg and Ca silicates at 25°C. *Chem. Geol.* **217**, 227–238.

Gough R. V., Chevrier V. F. and Tolbert M. A. (2016) Formation of liquid water at low temperatures via the deliquescence of calcium chloride: Implications for Antarctica and Mars. *Planetary and Space Science* **131**, 79–87.

Gómez F., Rodríguez-Manfredi J. A., Rodríguez N., Fernández-Sampedro M., Caballero-Castrejón F. J. and Amils R. (2012) Habitability: where to look for life? Halophilic habitats: earth analogs to study Mars habitability. *Planet. Space Sci.* **68**, 48–55.

Gooding J. L., Wentworth S. J. and Zolensky M. E. (1991) Aqueous alteration of the Nakhla meteorite. *Meteorit. Planet. Sci.* **26**, 135–143.

Gowda N. M. N., Naikar S. B. and Reddy G. K. N. (1984) Perchlorate ion complexes. *Adv. Inorgan. Chem.* **28**, 255–299.

Hall R. D. and Horn L. L. (1993) Rates of hornblende etching in soils in glacial deposits of the northern Rocky Mountains (Wyoming-Montana, USA): influence of climate and characteristics of the parent material. *Chem. Geol.* **105**, 17–29.

Hall R. D. and Michaud D. (1988) The use of hornblende etching, clast weathering, and soils to date alpine glacial and periglacial deposits: a study from southwestern Montana. *GSA Bull.* **100**, 458–467.

Harvey R. P., Wadhwa M., McSween H. Y. and Crozaz G. (1993) Petrography, mineral chemistry, and petrogenesis of Antarctic shergottite LEW88516. *Geochim. Cosmochim. Acta* **57**, 4769–4783.

Haskin L. A., Wang A., Jolliff B. L., McSween H. Y., Clark B. C., Des Marais D. J., McLennan S. M., Tosca N. J., Hurowitz J. A., Farmer J. D. and Yen A. (2005) Water alteration of rocks and soils on Mars at the Spirit rover site in Gusev crater. *Nature* **436**, 66–69.

Hausrath E. M. and Brantley S. L. (2010) Basalt and olivine dissolution under cold, salty, and acidic conditions: what can we learn about recent aqueous weathering on Mars? *J. Geophys. Rsh: Planets* **115**(E12).

Hausrath, E.M., Ming, D.W., Peretyazhko, T., Rampe, E.B., 2017. Using Reactive Transport Modeling to Understand Formation of the Stimson Sedimentary Unit and Altered Fracture Zones at Gale Crater, Mars.

Hoch A. R., Reddy M. M. and Drever J. I. (1996) The effect of iron content and dissolved O_2 on dissolution rates of clinopyroxene at pH 5.8 and 25°C: preliminary results. *Chem. Geol.* **132**, 151–156.

Högfeldt E. (1982) *Stability Constants of Metal-ion Complexes: Part A: Inorganic Ligands (Vol. 21)*. Pergamon Press, Elmsford, New York.

Icenhower J. P. and Dove P. M. (2000) The dissolution kinetics of amorphous silica into sodium chloride solutions: effects of temperature and ionic strength. *Geochim. Cosmochim. Acta* **64**, 4193–4203.

Karlsson M., Craven C., Dove P. M. and Casey W. H. (2001) Surface charge concentrations on silica in different 1.0 M metal-chloride background electrolytes and implications for dissolution rates. *Aquat. Geochem.* **7**, 13–32.

Klein, C., Hurlbut Jr., C.S. (1985) Manual of Mineralogy (after J. D. Dana), 20th Ed.. John Wiley and Sons, New York.

Klingelhöfer G. R. D. S., Morris R. V., Bernhardt B., Schröder C., Rodionov D. S., De Souza P. A., Yen A., Gellert R., Evlanov E. N., Zubkov B. and Foh J. (2004) Jarosite and hematite at Meridiani Planum from Opportunity's Mössbauer spectrometer. *Science* **306**, 1740–1745.

Knauss K. G., Nguyen S. N. and Weed H. C. (1993) Diopside dissolution kinetics as a function of pH, CO2, temperature, and time. *Geochim. Cosmochim. Acta* **57**, 285–294.

Kounaves, S.P., Hecht, M.H., Kapit, J., Godspodinova, K., DeFlores, L., Quinn, R.C., Boynton, W.V., Clark, B.C., Catling, D.C., Hredzak, P., Ming, D.W., Moore, Q., Shusterman, Stroble, J.S., West, S.J., Young, S.M.M., 2010a. Wet Chemistry experiments on the 2007 Phoenix Mars Scout Lander mission: data analysis and results. J. Geophys. Res. Lett., 115, E00E10, 10.1029/2009JE003424.

Kounaves S. P., Hecht M. H., Kapit J., Quinn R. C., Catling D. C., Clark B. C., Ming D. W., Godspodinova K., Hredzak P., McElhoney K. and Shusterman J. (2010b) Soluble sulfate in the Martian soil at the Phoenix landing site. *Geophys. Res. Lett.* **37**, L09201. https://doi.org/10.1029/2010GL042613.

Kraft, M.D., Michalski, J.R., Sharp, T.G., 2003. Effects of pure silica coatings on thermal emission spectra of basaltic rocks: considerations for Martian surface mineralogy. Geophys. Rsh. Let., 30(24). 10.1029/2003GL018848.

Le Truong G., De Laat J. and Legube B. (2004) Effects of chloride and sulfate on the rate of oxidation of ferrous ion by H_2O_2. *Water Res.* **38**(9), 2384–2394.

Langevin Y., Poulet F., Bibring J. P. and Gondet B. (2005) Sulfates in the north polar region of Mars detected by OMEGA/Mars Express. *Science* **307**, 1584–1586.

Lee M. R., MacLaren I., Andersson S. M. L., Kovacs A., Tomkinson T., Mark D. F. and Smith C. L. (2015) Opal-A in the Nakhla meteorite: a tracer of ephemeral liquid water in the Amazonian crust of Mars. *Meteor. Planet. Sci.* **50**, 1362–1377.

Ling Z. and Wang A. (2015) Spatial distributions of secondary minerals in the Martian meteorite MIL 03346, 168 determined by Raman spectroscopic imaging. *J. Geophys. Rsh: Planets* **120**, 1141–1159.

Martínez G. M., Renno N. O. and Elliott H. M. (2012) The evolution of the albedo of dark spots observed on Mars polar region. *Icarus* **221**, 816–830. https://doi.org/10.1016/j.icarus.2012.09.008.

McEwen A. S., Dundas C. M., Mattson S. S., Toigo A. D., Ojha L., Wray J. J. and Thomas N., et al. (2014) Recurring slope lineae in equatorial regions of Mars. *Nat. Geosci.* **7**, 53–58.

McEwen A. S., Ojha L., Dundas C. M., Mattson S. S., Byrne S. and Wray J. J., et al. (2011) Seasonal flows on warm Martian slopes. *Science* **333**, 740–743.

McLennan, S.M., Anderson, R.B., Bell, J.F., Bridges, J.C., Calef, F., Campbell, J.L., Des Marais, D.J., et al., Elemental geochemistry of sedimentary rocks at Yellowknife Bay, Gale crater, Mars. Science, **343**, 2013, 1244734.

McSween H. Y. (1994) What we have learned about Mars from SNC meteorites. *Meteoritics* **29**, 757–779.

McSween H. Y. (2002) The rocks of Mars, from far and near. *Meteor. Planet. Sci.* **37**(1), 7–25.

McSween H. Y., Arvidson R. E., Bell J. F., Blaney D., Cabrol N. A., Christensen P. R., Clark B. C., Crisp J. A., Crumpler L. S., Des Marais D. J. and Farmer J. D. (2004) Basaltic rocks analyzed by the Spirit rover in Gusev Crater. *Science* **305**(5685), 842–845.

McSween H. Y., Ruff S. W., Morris R. V., Gellert R., Klingelhoefer G., Christensen P. R., McCoy T. J., Ghosh A., Moersch J. M., Cohen B. A. and Rogers A. D. (2008) Mineralogy of volcanic rocks in Gusev crater, Mars: Reconciling Mössbauer, alpha particle X-ray spectrometer, and miniature thermal emission spectrometer spectra. *J. Geophys. Rsh: Planets* **113** (E6).

Morris R. V., Klingelhoefer G., SchrÃ¶der C., Fleischer I., Ming D. W., Yen A. S., Gellert R., Arvidson R. E., Rodionov D. S., Crumpler L. S. and Clark B. C. (2008) Iron mineralogy and aqueous alteration from Husband Hill through Home Plate at Gusev crater, Mars: Results from the MÃ¶ssbauer instrument on the Spirit Mars Exploration Rover. *Journal of Geophysical Research: Planets* **113**(E12).

Mikesell L. R., Schaetzl R. J. and Velbel M. A. (2004) Hornblende etching and quartz/feldspar ratios as weathering and soil development indicators in some Michigan soils. *Quat. Rsh* **62**, 162–171.

Miller J. L., Madden A. E., Phillips-Lander C. M., Pritchett B. N. and Madden M. E. (2016) Alunite dissolution rates: dissolution mechanisms and implications for Mars. *Geochim. Cosmochim. Acta* **172**, 93–106.

Millero F. J., Yao W. and Aicher J. (1995) The speciation of Fe(II) and Fe(III) in natural waters. *Mar. Chem.* **50**, 21–39.

Milliken R. E., Swayze G. A., Arvidson R. E., Bishop J. L., Clark R. N., Ehlmann B. L. and Mustard J. F., et al. (2008) Opaline silica in young deposits on Mars. *Geology* **36**, 847–850.

Mitchell J. L. and Christensen P. R. (2016) Recurring slope lineae and chlorides on the surface of Mars. *J. Geophys. Rsh.: Planets* **121**, 1411–1428.

Mittlefehldt D. W. (1994) ALH84001, a cumulate orthopyroxenite member of the Martian meteorite clan. *Meteoritics* **29**, 214–221.

Möhlmann D. and Kereszturi A. (2010) Viscous liquid film flow on dune slopes of Mars. *Icarus* **207**, 654–658.

Morgan B. and Lahav O. (2007) The effect of pH on the kinetics of spontaneous Fe(II) oxidation by O_2 in aqueous solution–basic principles and a simple heuristic description. *Chemosphere* **68** (11), 2080–2084.

Morris R. V., Klingelhoefer G., Bernhardt B., Schröder C., Rodionov D. S., De Souza P. A., Yen A., Gellert R., Evlanov E. N., Foh J. and Kankeleit E. (2004) Mineralogy at Gusev

Crater from the Mössbauer spectrometer on the Spirit Rover. *Science* **305**, 833–836.

Morris R. V., Klingelhoefer G., Schröder C., Rodionov D. S., Yen A., Ming D. W. and Bernhardt B., et al. (2006) Mössbauer mineralogy of rock, soil, and dust at Meridiani Planum, Mars: opportunity's journey across sulfate-rich outcrop, basaltic sand and dust, and hematite lag deposits. *J. Geophys. Res.: Planets* **111**(E12).

Mustard J. F., Poulet F., Gendrin A., Bibring J. P., Langevin Y., Gondet B., Mangold N., Bellucci G. and Altieri F. (2005) Olivine and pyroxene diversity in the crust of Mars. *Science* **307**, 1594–1597.

Mustard J. F., Poulet F., Head J. W., Mangold N., Bibring J. P., Pelkey S. M., Fassett C. I., Langevin Y. and Neukum G. (2007) Mineralogy of the Nili Fossae region with OMEGA/Mars Express data: 1. Ancient impact melt in the Isidis Basin and implications for the transition from the Noachian to Hesperian. *J. Geophys. Rsh. Planets* **112**(E8).

Nachon M., Clegg S. M., Mangold N., Schröder S., Kah L. C., Dromart G. and Le Mouélic S., et al. (2014) Calcium sulfate veins characterized by ChemCam/Curiosity at Gale crater, Mars. *J. Geophys. Rsh.: Planets* **119**, 1991–2016.

Niles P. B., Michalski J., Ming D. W. and Golden D. C. (2017) Elevated olivine weathering rates and sulfate formation at cryogenic temperatures on Mars. *Nat. Commun.* **8**(1), 998.

Nyquist L. E., Bogard D. D., Shih C. Y., Greshake A., Stöffler D. and Eugster O. (2001) Ages and geologic histories of Martian meteorites. In *Chronology and Evolution of Mars*. Springer, Netherlands, pp. 105–164.

Oelkers E. H. and Schott J. (2001) An experimental study of enstatite dissolution rates as a function of pH, temperature, and aqueous Mg and Si concentration, and the mechanism of pyroxene/pyroxenoid dissolution. *Geochim. Cosmochim. Acta* **65**, 1219–1231.

Ojha L., McEwen A., Dundas C., Byrne S., Mattson S., Wray J. and Schaefer E., et al. (2014) HiRISE observations of recurring slope lineae (RSL) during southern summer on Mars. *Icarus* **231**, 365–376.

Ojha L., Wilhelm M. B., Murchie S. L., McEwen A. S., Wray J. J., Hanley J. and Chojnacki M., et al. (2015) Spectral evidence for hydrated salts in recurring slope lineae on Mars. *Nat. Geosci.* **8**, 829–832.

Olsen A. A., Hausrath E. M. and Rimstidt J. D. (2015) Forsterite dissolution rates in Mg-sulfate-rich Mars-analog brines and implications of the aqueous history of Mars. *J. Geophys. Rsh.: Planets* **120**, 388–400. https://doi.org/10.1002/2014JE004664.

Osterloo M. M., Anderson F. S., Hamilton V. E. and Hynek B. M. (2010) Geologic context of proposed chloride-bearing materials on Mars. *J. of Geophys. Rsh. Planets* **115**(E10).

Osterloo M. M., Hamilton V. E., Bandfield J. L., Glotch T. D., Baldridge A. M., Christensen P. R., Tornabene L. L. and Anderson F. S. (2008) Chloride-bearing materials in the southern highlands of Mars. *Science* **319**, 1651–1654.

Phillips-Lander C. M., Fowle D. A., Taunton A., Hernandez W., Mora M., Moore D., Shinogle H. and Roberts J. A. (2014) Silicate dissolution in Las Pailas thermal field: implications for microbial weathering in acidic volcanic hydrothermal spring systems. *Geomicro J.* **31**, 23–41.

Phillips-Lander C. M., Legett C., Elwood Madden A. S. and Elwood Madden M. E. (2017) Can we use pyroxene weathering textures to interpret aqueous alteration conditions? Yes and No. *Am. Mineral.* **102**, 1915–1921.

Phillips-Lander C. M., Parnell S. R., McGraw L. E. and Elwood Madden M. E. (2018) Carbonate dissolution rates in high salinity brines: Implications for post-Noachian chemical weathering on Mars. *Icarus 307*, 281–293.

Pritchett B. N., Elwood Madden M. E. and Madden A. S. (2012) Jarosite dissolution rates and maximum lifetimes in high salinity brines: Implications for Earth and Mars. *Earth Planet. Sci. Let.* **357**, 327–336.

Ragnarsdóttir K. V. (1993) Dissolution kinetics of heulandite at pH 2–12 and 25 C. *Geochim. Cosmochim. Acta* **57**(11), 2439–2449.

Rampe E. B., Lapotre M., Bristow T. F., Arvidson R. E., Morris R. V., Achilles C. N. and Vaniman D. T., et al. (2018) Sand mineralogy within the Bagnold Dunes, Gale crater, as observed in situ and from orbit. *Geophys. Res. Lett*.

Rampe E. B., Ming D. W., Blake D. F., Bristow T. F., Chipera S. J., Grotzinger J. P. and Achilles C. N., et al. (2017) Mineralogy of an ancient lacustrine mudstone succession from the Murray formation, Gale crater,Mars. *Earth and Planet. Sci. Lett.* **471**, 172–185.

Rennó N. O., Bos B. J., Catling D., Clark B. C., Drube L., Fisher D., Goetz W., Hviid S. F., Keller H. U., Kok J. F. and Kounaves S. P. (2009) Possible physical and thermodynamical evidence for liquid water at the Phoenix landing site. *J. Geophys. Rsh: Planets* **114**(E1). https://doi.org/10.1029/2009JE003362.

Ruiz-Agudo E., Putnis C. V., Jiménez-López C. and Rodriguez-Navarro C. (2009) An atomic force microscopy study of calcite dissolution in saline solutions: the role of magnesium ions. *Geochim. Cosmochim. Acta* **73**, 3201–3217.

Savage D., Rochelle C., Moore Y., Milodowski A., Bateman K., Bailey D. and Mihara M. (2001) Analcime reactions at 25–90 C in hyperalkaline fluids. *Mineral. Magaz.* **65**(5), 571–587.

Schaetzl R. J., Mikesell L. R. and Velbel M. A. (2006) Soil characteristics related to weathering and pedogenesis across a geomorphic surface of uniform age in Michigan. *Phys. Geogr.* **27**, 170–188.

Schott J. and Berner R. A. (1985) Dissolution mechanisms of pyroxenes and olivines during weathering. *Chem. Weath.* **149**, 35–53.

Schott J., Berner R. A. and Sjöberg E. L. (1981) Mechanism of pyroxene and amphibole weathering—I. Experimental studies of iron-free minerals. *Geochim. Cosmochim. Acta* **45**, 2123–2135.

Sidhu P. S., Gilkes R. J., Cornell R. M., Posner A. M. and Quirk J. P. (1981) Dissolution of iron oxides and oxyhydroxides in hydrochloric and perchloric acids. *Clays Clay Miner.* **29**, 269–276.

Squyres S. W., Arvidson R. E., Bell J. F., Brückner J., Cabrol N. A., Calvin W., Carr M. H., Christensen P. R., Clark B. C., Crumpler L. and Des Marais D. J. (2004) The Opportunity Rover's Athena science investigation at Meridiani Planum, Mars. *Science* **306**, 1698–1703.

Squyres S. W., Arvidson R. E., Ruff S., Gellert R., Morris R. V., Ming D. W. and McLennan S. M., et al. (2008) Detection of silica-rich deposits on Mars. *Science* **320**, 1063–1067.

Steiner M. H., Hausrath E. M., Madden M. E., Tschauner O., Ehlmann B. L., Olsen A. A., Gainey S. R. and Smith J. S. (2016) Dissolution of nontronite in chloride brines and implications for the aqueous history of Mars. *Geochim. Cosmochim. Acta* **195**, 259–276.

Sutter B., Mcadam A. C., Mahaffy P. R., Ming D. W., Edgett K. S., Rampe E. B. and Steele A., et al. (2017) Evolved gas analyses of sedimentary rocks and eolian sediment in Gale Crater, Mars: results of the Curiosity rover's sample analysis at Mars instrument from Yellowknife Bay to the Namib Dune. *JGR: Planets* **122**(12), 2574–2609.

Tanaka M. and Takahashi K. (2005) Characterization of silicate complexes in aqueous sodium sulfate solutions by FAB-MS. *J. Sol. Chem.* **34**, 617–630.

Thomas-Keprta, K.L., Wentworth, S.J., McKay, D.S., Gibson, E. K., 2000. Field emission gun scanning electron (FEGSEM) and transmission electron (TEM) microscopy of phyllosilicates in martian meteorites ALH84001, Nakhla, and Shergotty. Lunar and Planet. Sci. XXXI. Lunar Planet. Inst., Houston. #1690 (abstr.).

Toner J. D. and Catling D. C. (2017) A low-temperature thermodynamic model for the Na-K-Ca-Mg-Cl system incorporating new experimental heat capacities in KCl, $MgCl_2$, and $CaCl_2$ solutions. *J. Chem. Eng. Data* **62**(3), 995–1010.

Treiman A. H. (2005) The nakhlite meteorites: Augite-rich igneous rocks from Mars. *Chem. der Erde-Geochem.* **65**, 203–270.

Treiman A. H., Barrett R. A. and Gooding J. L. (1993) Preterrestrial aqueous alteration of the Lafayette (SNC) meteorite. *Meteoritics* **28**, 86–97.

Treiman A. H., Bish D. L., Vaniman D. T., Chipera S. J., Blake D. F., Ming D. W., Morris R. V., Bristow T. F., Morrison S. M., Baker M. B. and Rampe E. B. (2016) Mineralogy, provenance, and diagenesis of a potassic basaltic sandstone on Mars: CheMin X-ray diffraction of the Windjana sample (Kimberley area, Gale Crater). *J. Geophys. Rsh: Planets* **121**, 75–106.

Vaniman D. T., Bish D. L., Ming D. W., Bristow T. F., Morris R. V., Blake D. F., Chipera S. J., Morrison S. M., Treiman A. H., Rampe E. B. and Rice M. (2013) Mineralogy of a mudstone at Yellowknife Bay, Gale crater. *Mars. Science* **343**, 1243480.

Velbel M. A. (2007) Surface textures and dissolution processes of heavy minerals in the sedimentary cycle: examples from pyroxenes and amphiboles. *Develop. Sedimentol.* **58**, 113–150.

Velbel M. A. (2012) Aqueous alteration in Martian meteorites: Comparing mineral relations in igneous-rock weathering of Martian meteorites and in the sedimentary cycle of Mars. In Sedimentary Geology of Mars. *Soc. Sedim. Geol. Spec. Publ.* **102**, 97–117.

Velbel M. A. and Barker W. W. (2008) Pyroxene weathering to smectite: conventional and cryo-field emission scanning electron microscopy, Koua Bocca ultramafic complex, Ivory Coast. *Clays Clay Miner.* **56**, 112–127.

Velbel M. A. and Losiak A. I. (2010) Denticles on chain silicate grain surfaces and their utility as indicators of weathering conditions on Earth and Mars. *J. Sed. Rsh* **80**, 771–780.

Wentworth S. J. and Gooding J. L. (1994) Carbonates and sulfates in the Chassigny meteorite: further evidence for aqueous chemistry on the SNC parent planet. *Meteoritics* **29**, 860–863.

White A. F. and Yee A. (1985) Aqueous oxidation-reduction kinetics associated with coupled electron-cation transfer from iron-containing silicates at 25°C. *Geochim. Cosmochim. Acta* **49** (5), 1263–1275.

Yen A. S., Ming D. W., Vaniman D. T., Gellert R., Blake D. F., Morris R. V. and Treiman A. H., et al. (2017) Multiple stages of aqueous alteration along fractures in mudstone and sandstone strata in Gale Crater, Mars. *EPSL* **471**, 186–198.

Associate editor: Jeffrey G. Catalano